Summer 8-2019

Understanding Volume Transport in the Jordan River: an Application of the Navier-Stokes Equations

Gwyneth E. Roberts
University of Maine, gwyneth.roberts@maine.edu

UNDERSTANDING VOLUME TRANSPORT IN THE JORDAN RIVER: AN APPLICATION OF THE NAVIER-STOKES EQUATIONS

by

Gwyneth E. Roberts

Thesis Submitted in Partial Fulfillment of the
Requirements for a Degree with Honors
(Mathematics)

The Honors College

University of Maine

August 2019

Advisory Committee:

- Dr. Thomas Bellsky, Assistant Professor of Mathematics, Co-Advisor
- Dr. Lauren Ross, Assistant Professor of Civil Engineering, Co-Advisor
- Dr. Sean Smith, Associate Professor of Earth & Climate Sciences
- Dr. Neil Fisher, Lab Manager & Instructor
- Dr. François G. Amar, Professor of Chemistry & Dean of the Honors College

ABSTRACT

This study aims to characterize the circulation patterns in short and narrow estuarine systems on various temporal scales to identify the controls of material transport. In order to achieve this goal, a combination of *in situ* collected data and analytical modeling was used. The model is based on the horizontal Reynolds Averaged Navier-Stokes equations in the shallow water limit with scaling parameters defined from the characteristics of the estuary. The *in situ* measurements were used to inform a case study, seeking to understand water level variations and tidal current velocity patterns in the Jordan River and to improve understanding of the hydrodynamic conditions and their implications for water quality. The Jordan River in Trenton, Maine is host to commercial mussel harvesting activities. These local aquaculture operations are susceptible to point source pollution and freshwater runoff induced closures, which are inherently linked to the dynamics of the estuary. Preliminary results of the data analysis indicate that ebb velocities are dominant in the intra-tidal dynamics, suggesting that subtidal (transport) velocities will be prominent in this system. Model results for subtidal flows show that there is outflow over the shoals and inflow over the channel driven by a combination of advection and Stokes drift. This pattern indicates that pollutants introduced to the system near the banks (from land-based sources) will be advected out of the system while pollutants introduced in the center (or from the seaward boundary) will be advected into the system. Thus, land-based pollutants will spend less time within the estuary. These results can be used to inform management decisions to minimize closure time throughout the harvest season.

TABLE OF CONTENTS

1 Introduction....1
1.1 Background....1
1.1.1 Estuaries....1
1.1.2 Tidal Flow....2
1.1.3 Subtidal Flow....3
1.2 Motivation....3
2 Methods....6
2.1 Study area....6
2.2 Data Collection....7
2.3 Data Processing....9
3 Model and Solutions....11
3.1 First Order Equations....13
3.2 Second Order Equations....24
4 Understanding volume transport....30
4.1 Data Analysis....30
4.1.1 Bathymetry....30
4.1.2 Salinity Structure....31
4.1.3 Water Level....32
4.1.4 Velocity....33
4.2 Subtidal Flows and Transport....34
4.3 Discussion....36
4.4 Gradients....39
5 Conclusions....42
References....44
Author's Biography....46

TABLE OF FIGURES

Figure 1.....2
Figure 2.....4
Figure 3.....7
Figure 4.....8
Figure 5.....11
Figure 6.....31
Figure 7.....32
Figure 8.....32
Figure 9.....33
Figure 10.....34
Figure 11.....35
Figure 12.....37
Figure 13.....40

CHAPTER 1

INTRODUCTION

1.1 Background

1.1.1 Estuaries

An estuary is where fresh and saltwater meet and mix. The term refers to a semi-enclosed basin fed by land derived freshwater which is in free exchange with the ocean at one end (Cameron & Pritchard, 1963). Estuaries are defined as the extent to which the tide influences water levels in a river. The slightly saline (brackish) water that forms as a result of this mixing plays host to many marine species (NOAA, 2018). They provide ecosystem services to their local communities, acting as buffer zones in the event of storms and flooding and preventing coastal erosion, and supporting fisheries that have historically been an economically important resource.

There are four geomorphological classifications of estuarine systems: coastal floodplain, tectonic, bar built, and fjord. Coastal floodplain systems are most common in temperate latitudes. These systems form when sea-levels rise rapidly, as they did at the end of the last glacial maximum (approximately 15,000 years ago), flooding existing coastal rivers (Pritchard, 1952). Figure 1 shows a typical schematic of this type of estuary.

As in all estuaries, the mouth is the boundary with free exchange with the ocean, the head is the landward boundary where freshwater commonly enters the system from a riverine source. These systems can vary in length from a few hundred meters to a few hundred kilometers, and can also be classified based on salinity structure, formation, and relative freshwater inputs (Valle-Levinson, 2010).

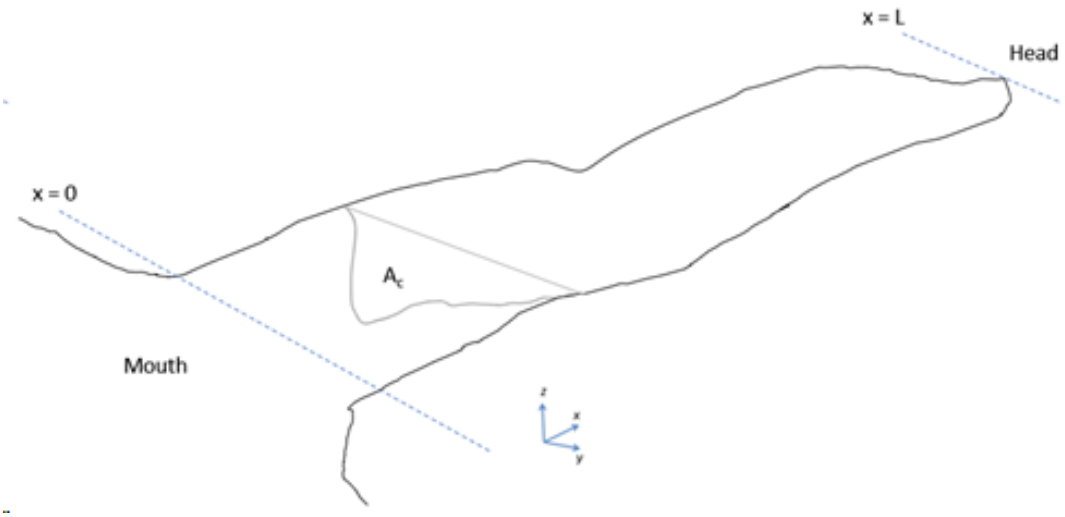

Figure 1: Typical morphology of a coastal plain estuary. The position along channel is measured by x, and the total length of the system is L . The cross-sectional flow area, dependent on the water level (ζ), is A_c .

1.1.2 Tidal Flow

Tides are the product of the gravitational pull of the Moon and the Sun, and also due to the net centrifugal force exerted as the Earth and Moon both rotate around a common center of mass between the two bodies as seen in Figure 2 (NOAA). This centrifugal force is of equal magnitude at all points along the axis of revolution and is directed away from the common center, and points towards the axis of revolution towards the poles. The gravitational pull of the Moon on the Earth is stronger at the surface to which it is closer (facing), thus a net tidal force outward from the surface is created. At the surface facing the moon, the centrifugal force remains constant, but the gravitational pull of the moon is diminished with distance. Thus, a net tidal force outward in the opposite direction is created. These tidal forces create 'bulges' of ocean water, and as the Earth rotates underneath them, the sea surface rises and falls from a constant reference point on Earth. The primary driver of water (and thus suspended particle) movement in estuaries is the periodic rise and fall of the sea surface due to tides (Geyer & MacCready, 2014).

1.1.3 Subtidal Flow

Pollutant and particulate matter persist far longer than the period of a single tidal wave (12-24 hours). This is because tidal excursion (the net distance a particle travels over a single tidal period) is typically not large enough to advect particles out of an estuary over the course of one tidal cycle (Geyer & Signell, 1992). Subtidal flows are generated when there is net movement of a fluid particle within one tidal cycle, resulting in long term net motion over the span of multiple tidal cycles.

Subtidal flows have multiple driving forces including morphology (Dronkers, 1986), salinity gradients (Geyer & MacCready, 2014), wind (Huijits et al. 2011), and freshwater discharge from the landward boundary. For pollutant and particulate matter, transport is governed by these subtidal mechanisms (Li & O'Donnell 2005).

1.2 Motivation

The goal of this study is to contribute to the understanding of intratidal and subtidal flow dynamics in low-inflow, dynamically small systems (with a ratio of ${}^{4L}/\lambda < 0.6$ as defined in Li & O'Donnell 2005, with L being the length of the estuary and λ being the wavelength of the tidal wave), using the Jordan River as a study site. This will be accomplished by answering two specific research objectives. The first of which is to determine if tidal asymmetries in current velocities are present in a dynamically small estuary with low river input.

The second is to identify the drivers of subtidal flow patterns and link these patterns to intra-tidal asymmetries in the velocities. The objectives will be addressed using a combination of *in situ* collected data and analytical modeling. This paper will characterize the residual velocities to form a better understanding of fluid transport (and thus material transport) in a dynamically small estuarine system.

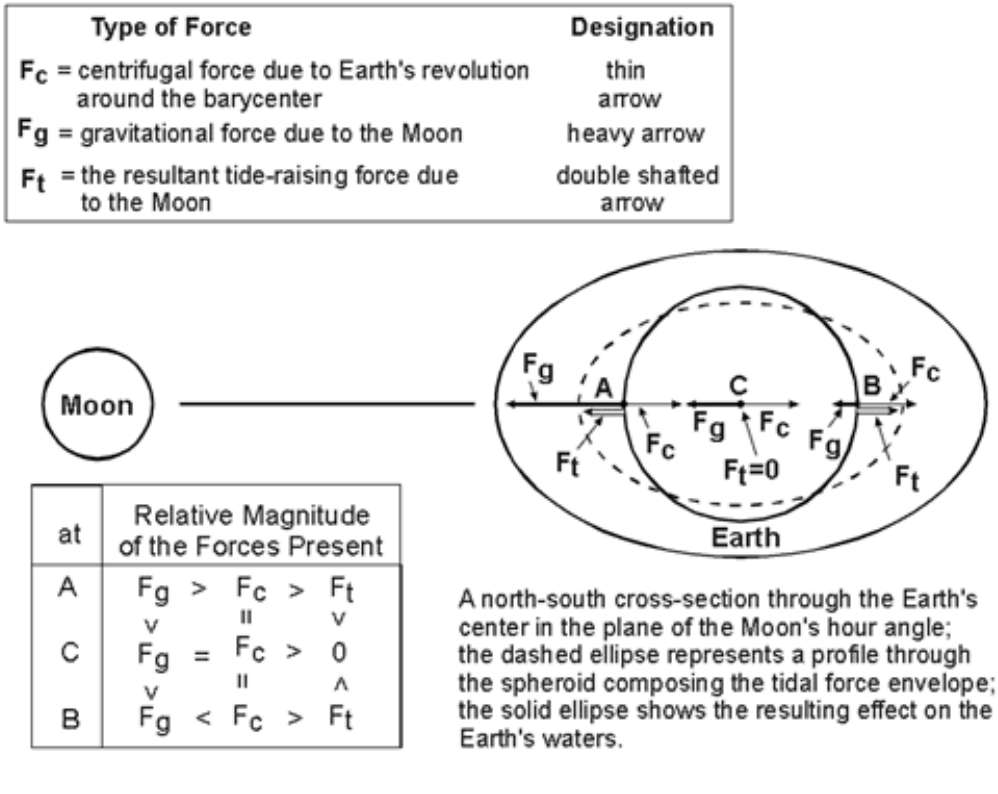

Figure 2: Forcing mechanisms of global tides. Both gravitational and centrifugal forces create periodic change in water level by causing ocean water to bulge in areas under these influences (NOAA, 2018).

Tidal characteristics such as water level elevation and axial velocity in estuaries have been previously studied using analytical models for various morphology classes (Friedrichs, 2010). The inception of subtidal flow analysis defined and derived the 'time mean equations' which describe the magnitude of axial and vertical tidal velocity over one or more tidal cycles, showing a characteristic inflow at depth and outflow at the surface (Pritchard, 1956). However, this was dependent on salinity gradients caused by non-insignificant riverine input. Various model studies quantify subtidal flow in well-mixed systems but are applied to large estuaries (Li & Valle-Levinson 1999, Li & O'Donnell 2005).

There are many approaches to understand the circulation patterns driving subtidal flows within an estuary. The first are numerical models, which use

calculations and visualizations to recreate each estuarine field as realistically as possible. The Navier-Stokes equations are discretized to allow for multiple iterations with small time steps, which are run through the constructed field. Numerical models are useful in capturing high resolution flow fields and modeling small scale changes in velocity. Dynamic properties can be modelled with precision to quantify properties including both tidal and subtidal flows, salinity structure throughout time, and tidal characteristics (Warner et al, 2005). This approach can be used to compare long and short systems in terms of the tidal wave and more sensitive mechanisms such as vertical salinity gradient (Chen et al. 2011).

The outputs obtained from these models are often detailed. However, analytical models can study how different parameters such as basin length, depth, friction, etc. alter tidal and subtidal flow in a systematic way. Such models require 'pen-and-paper' derivations, beginning with governing physical equations and balances. From these foundational equations, a variety of mathematical methods are employed to obtain closed-form solutions specific to certain systems. These models require that the system be represented by idealized parameters, in order to make derivations possible and practicable. This leads to results that are less minutely detailed than those from a numerical model. However, despite the sacrifice of small-scale precision, we are able to isolate the physical processes responsible for the modeled circulation and compare their relative impacts overall (Huijts et al, 2009).

This thesis will first describe the study area, data collection, and data processing techniques in Chapter 2. The two-dimensional model from Li & O'Donnell describing subtidal flow will be introduced, with appropriate assumptions, parameters, and derivations in Chapter 3. Results of the data analysis and case study isolating the mechanisms driving subtidal flows will be presented in Chapter 4, with discussion in Chapter 5.

CHAPTER 2

METHODS

2.1 Study Area

In order to derive analytical solutions, a field study was conducted in Trenton, Maine to collect parameters such as axial and lateral velocity data, water level elevation changes, and density gradients. This system was chosen due to its importance to the nearby operations of Acadia Aquafarms. They maintain cages seeded with blue mussels just outside the mouth of the estuary (the portion closest to the open ocean). The physics of this system has not been widely studied, presumably because it is remarkably small. Because of the sedentary nature of the mussels, both caged and wild, the hydrodynamics of the estuary play a role in regulating exposure to potential pollutants and runoff (Viarengo & Canesi, 1991). The Maine Department of Marine Resources (MEDMR) currently mandates shellfish harvesting closure procedures to minimize the public's exposure to pollutants. Currently, a 2-inch rainfall event spanning 24 hours or less triggers a mandatory 2-week closure for all affected areas. This is applied universally across the state, despite substantial differences in the hydrology and hydraulics relative to coastal settings in the state.

The study area is located 2 km north of Mount Desert Island in Trenton, Maine in the Jordan River Estuary (Figure 3). Data from the National Oceanic and Atmospheric Association (NOAA) weather buoy off the coast of nearby Bar Harbor shows that the mean tidal range in Frenchman Bay is 3.2 meters (NOAA, 2018). The length (L) is approximately 4.88 km from mouth to head, the average width along the system is 142 meters, and the average depth is 5.5 meters.

2.2 Data Collection

In order to measure the water level elevation throughout multiple tidal cycles, three Solinst Levelogger pressure sensors were deployed along the estuary (see figure 3). Additionally, one Solinst barometric pressure gage was stationed onshore to correct for atmospheric changes. These devices recorded absolute pressure beneath the surface and temperature at 10-minute intervals. Water pressure readings (corrected with barometric readings) were used to calculate the depth of the water column above each submerged sensor, resulting in the wave seen in figure 3. These were left in the estuary, continuously collecting data, from the 16th of August to the 13th of September 2018.

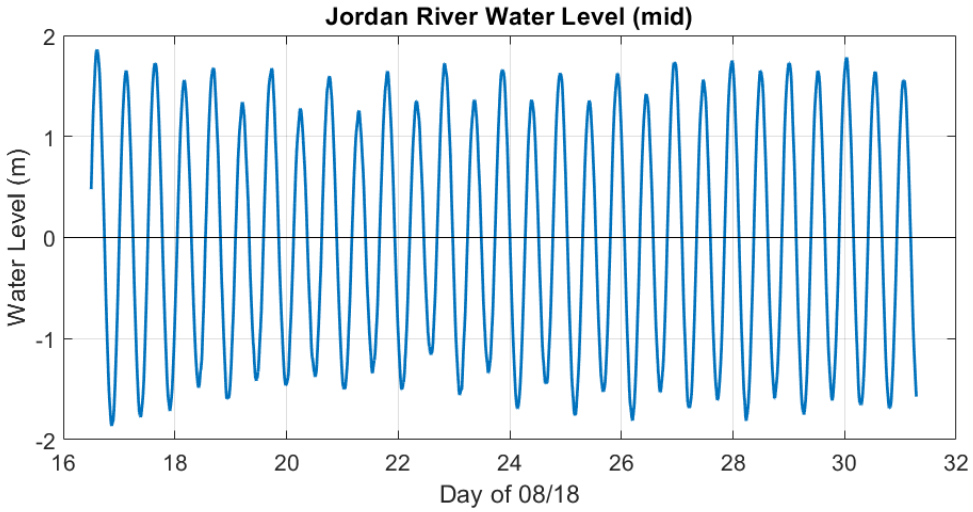

Figure 3: Varying water level in the Jordan River from pressure sensor readings closest to the velocity transect of interest (transect 1).

During a sampling period of approximately 13 hours on September 13, 2018, Acoustic Doppler Current Profiler (ADCP) velocity profiles were collected across two sections in the estuary. A 1200 kHz RDI ADCP was used, taking 1 reading every 2 seconds, at 25 cm intervals throughout the water column. Transect 1 was nearer the head of the estuary (1566 meters from the mouth) and transect 2 was

nearer the mouth of the system (1106 meters from the mouth). The bottom 10% of the profiles were eliminated from analysis to reduce side-lobe effects. A GPS unit was mounted on the ADCP device to track the location of the instrument. The locations of the transects were in the lower portion of the estuary because the channel is extremely shallow towards the head. During low tide, it is difficult to navigate, even within the central channel. Thus, taking a sweeping transect of the entire system during that time would have proven impossible, as the shoals were too shallow for even our small skiff. A total of 27 transects were taken at the head station over the course of one semidiurnal tidal cycle (approximately 12.42 hours). An entire tidal cycle is needed to be able to isolate the velocities working over timescales longer than that of the tide.

A Sontek Conductivity, Temperature, and Depth (CTD) profiler recorded measurements of salinity throughout depth during each transect (see Figure 4). The device sampled every 0.3 meters, at a rate of 5 Hz, and can report salinity to 0.1 psu accuracy and temperature to 0.05° C accuracy. A GPS unit housed in the system ensures that profiles are referenced using both time and location.

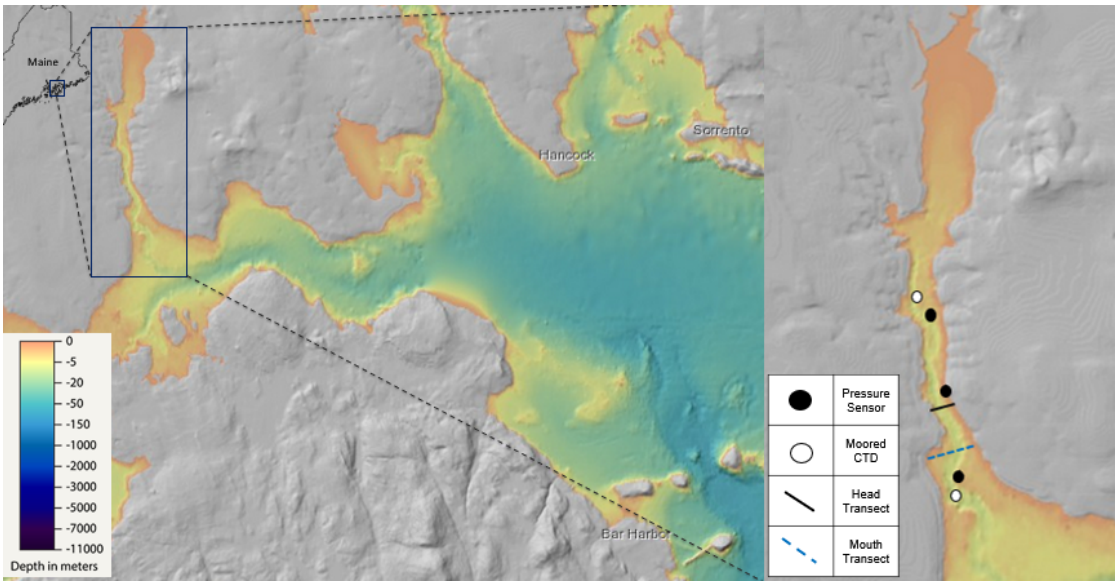

Figure 4: Study site and sampling locations at Jordan River in Trenton, Maine. The Mount Desert Narrows and Frenchman Bay are to the south.

Much of the site selected for transect 2 was too shallow to traverse at low tide, thus transect 1 (nearer the head) more accurately describes the magnitude of residual flows across the entire system. Thus, from this point forwards, we will be focusing on this transect to fit our model.

2.3 Data Processing

The water level elevation data measured the height of water above each sensor at 10-minute intervals. The heights were corrected for the dimensions of the anchoring system laid on the bottom of the estuary. Measurements obtained by the pressure sensors was not able to be given a true elevation due to limitations of the sighting equipment. This does not allow for analysis of a residual water level elevation (ζ'). However, the data were corrected around a mean unique to each sensor location (to achieve a wave oscillating about 0) which was used to quantify tidal amplitude at each location (the difference between high and low water). These data also underwent a least squares fit, isolating the components of the water level variation attributed to different tidal harmonics. For example, water level elevation can be decomposed as follows:

$$\zeta(x) = \zeta'(x) + \zeta_{M2}\cos(\omega_{M2}t + \phi_{M2}) + \zeta_{M4}\cos(\omega_{M4}t + \phi_{M4})...$$

where ζ is total water level elevation, ζ_0 is the residual water level elevation, ω_{M2} is the tidal frequency of the $M2$ harmonic (with a period of 12.42 hours), ζ_{M2} is the water level elevation driven by the $M2$ constituent, ω_{M4} is the tidal frequency of the $M4$ constituent (with a period of 6.21 hours), ζ_{M4} is the water level elevation driven by the $M4$ constituent, and t is time. The $M2$ constituent is the principal lunar semidiurnal harmonic, caused by the gravitational pull of the moon (see figure 2). It is in most cases the dominant tidal harmonic causing high and low water throughout the day. The $M4$ constituent is known as an overtide and is a result of

the $M2$ constituent interacting with itself and producing nonlinearities in shallow conditions, and thus producing subtidal flows (Andersen, 2003).

The velocity measurements were initially combed for bad data, with a 90% threshold eliminating equipment outliers (data exceeding 10% of the maximum flow were eliminated). The data were then passed through processing code to rotate to a primary axis using regression analysis. This process used the ADCP bottom tracking and GPS data to correct for the speed and heading of the vessel during transects, leaving only the movement of the fluid underneath (Joyce, 1989). The data was then interpolated to a uniform grid, with 100 cross channel distance bins at 1.7 meter intervals and 27 depth bins at 0.25 meters. Then, a least squares fit was applied to the velocity profile data obtained by the ADCP sampling isolating axial (u) and lateral (v) components of the flow (Thompson & Emery, 2014). This method fits the data to a series of theoretical tidal curves and allows us to isolate the effects of different harmonics. A residual term is also isolated (similar to the process for isolating ζ'), that describes flow not attributed to lower level tidal forcing.

CHAPTER 3

MODEL AND SOLUTIONS

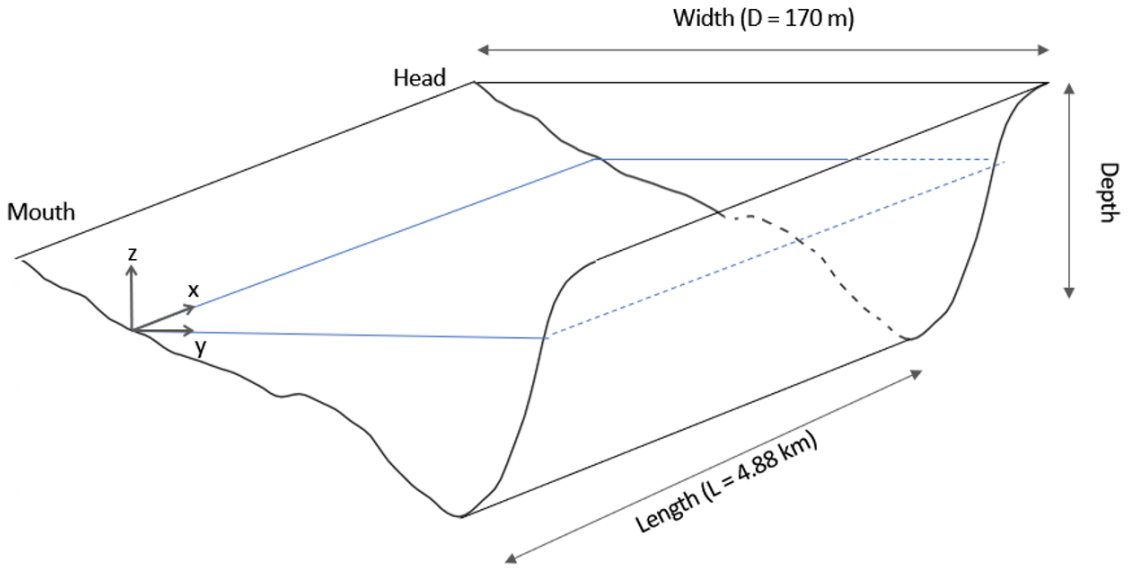

Figure 5: Model domain with bathymetry from data, and an idealized along channel geometry. Smoothed bathymetry imposed on a rectangular channel with no axial variation in depth. Note that $z = 0$ is located at the mean water level.

The idealized two-dimensional model used in this study is based on work presented in Li & O'Donnell 2005. The assumptions that are made in the derivation of these solutions are: the channel is narrow and shallow, there are no density gradients (i.e. neglecting vertical variations in salinity and therefore assuming a homogeneous system), and no Coriolis effects. The practical definition of narrow is a channel in which the lateral variation in the tidal amplitude (ζ_0) is much less than the mean of the tidal amplitude (ζ_0) (Li & Valle-Levinson, 1999). We can classify the Jordan as narrow because the system is less than a kilometer wide, the threshold being on the order of 10 km. During the sampling period, river discharge at the head was extremely low (with a monthly average of 0.043 $^{m^3}/_s$). This lends itself well to our homogeneous system assumption. We can also see in figure 7, there

is little vertical variation in salinity measurements during Fall sampling, and we can classify this system as well-mixed. Also, to be noted is that for values of axial flow, positive values denote landward flow and negative values denote seaward flow.
We begin with the Navier Stokes equations in the Shallow water limit:

$$\frac{\partial u}{\partial t} + u\frac{\partial u}{\partial x} + v\frac{\partial u}{\partial y} = -g\frac{\partial \zeta}{\partial x} - \frac{C_D u\sqrt{u^2+v^2}}{h+\zeta}$$
$$\frac{\partial v}{\partial t} + u\frac{\partial v}{\partial x} + v\frac{\partial v}{\partial y} = -g\frac{\partial \zeta}{\partial x} - \frac{C_D v\sqrt{u^2+v^2}}{h+\zeta}$$
$$\frac{\partial \zeta}{\partial t} + \frac{\partial (h+\zeta)u}{\partial x} + \frac{\partial (h+\zeta)v}{\partial y} = 0,$$

where u is axial velocity, v is lateral velocity, t is time, x is position along the channel, y is position across the channel, ζ is the water level elevation, h is the depth which varies across the channel (this can be any arbitrary function $h(y)$ of the across channel position), g is the gravitational constant, and C_D is the bottom drag coefficient. It is to be noted that the mouth of the estuary is $x = 0$ and the head is $x = L$, where L is the length of the channel. Similarly, the cross-channel profile varies from 0 to D bank to bank, where D is the width of the channel, constant along x (see Figure 5).

Firstly, the friction terms in the shallow water equations ($\frac{C_D u\sqrt{u^2+v^2}}{h+\zeta}$ and $\frac{C_D v\sqrt{u^2+v^2}}{h+\zeta}$) are each represented by their Fourier decomposition to linearize this highly non-linear term, thus making an analytical solution possible. This is a process much too long to describe in this paper, that can be found in Parker 1984. These can now be expressed as

$$\frac{\partial u}{\partial t} + u\frac{\partial u}{\partial x} + v\frac{\partial u}{\partial y} = -g\frac{\partial \zeta}{\partial x} - \beta\frac{u}{h} + \frac{\beta}{h^2}u\zeta$$
$$\frac{\partial v}{\delta t} + u\frac{\partial v}{\delta x} + v\frac{\partial v}{\partial y} = -g\frac{\delta \zeta}{\partial x} - \beta\frac{v}{h} + \frac{\beta}{h^2}v\zeta$$
$$\frac{\partial \zeta}{\partial t} + \frac{\partial (h+\zeta)u}{\partial x} + \frac{\partial (h+\zeta)v}{\partial y} = 0, \qquad (1)$$

where $\beta = {}^{8C_D U_0}/_{3\pi}$ and U_0 is the magnitude of the axial velocity. We break each tidally dependent variable ($u,\ v,\ \zeta$) into first, second, and higher order constituents. For example, $u = u_1 + u_2...$, where u_1 represents the first order (tidally forced) constituent of the axial flow (similarly for v_1 and ζ_1). Then, u_2 represents higher order subtidal axial flow (similarly for subtidal lateral flow v_2 and subtidal water level elevation ζ_2).

3.1 First Order Equations

First, we must non-dimensionalize these equations. This process scales each term, allowing for analysis of their relative impacts on flow, and further isolation of the most influential among them. We do this by applying the following normalized identities as presented in Li & O'Donnell, 2005:

$$
\begin{array}{lll}
u = \hat{u}\ U_0 & y = \hat{y}\ D & T = {}^{2\pi}/_{\sigma} \\
v = \hat{v}\ V_0 & h = \hat{h}\ h_0 & U_0 = \zeta_0\ \sqrt{{}^{g}/_{h_0}} \\
\zeta = \hat{\zeta}\ \zeta_0 & t = \hat{t}\ {}^{1}/_{\sigma} & V_0 = \epsilon\ \sigma\ D \\
x = \hat{x}\ L_0 & L_0 = {}^{\lambda}/_{2\pi} = {}^{T\ \sqrt{g\ h_0}}/_{2\pi} &
\end{array}
\tag{2}
$$

with ($\hat{x}$) denoting non-dimensional variables, with $U_0,\ V_0,\ \zeta_0,\ L_0,\ h_0$, denoting scales for axial velocity, lateral velocity, water level elevation, system length, undisturbed depth, and with σ, and λ denoting the angular frequency and wavelength of the tide respectively.

In order to isolate the first order (semi-diurnal tidally forced) terms from this equation, we substitute identities in equations (2) into the first equation in (1), isolating the coefficients. This gives us the following:

$$\Big(U_0\ \sigma\Big)\frac{\partial \hat{u}}{\partial \hat{t}} + \Big(\frac{U_0^2}{L_0}\Big)\hat{u}\frac{\partial \hat{u}}{\partial \hat{x}} + \Big(\frac{V_0 U_0}{D}\Big)\hat{v}\frac{\partial \hat{u}}{\partial \hat{y}} = -\Big(\frac{\zeta_0}{L_0}\Big)g\frac{\partial \hat{\zeta}}{\partial \hat{x}} - \Big(\frac{U_0}{h_0}\Big)\beta\frac{\hat{u}}{\hat{h}} + \Big(\frac{U_0\zeta_0}{h_0^2}\Big)\frac{\beta}{\hat{h}^2}\hat{u}\hat{\zeta}.$$

Dividing by $U_0\ \sigma$ gives:

$$\frac{\partial \hat{u}}{\partial \hat{t}} + \Big(\frac{U_0}{L_0\sigma}\Big)\hat{u}\frac{\partial \hat{u}}{\partial \hat{x}} + \Big(\frac{V_0}{D\sigma}\Big)\hat{v}\frac{\partial \hat{u}}{\partial \hat{y}} = -\Big(\frac{\zeta_0}{L_0U_0\sigma}\Big)g\frac{\partial \hat{\zeta}}{\partial \hat{x}} - \Big(\frac{1}{h_0\sigma}\Big)\beta\frac{\hat{u}}{\hat{h}} + \Big(\frac{\zeta_0}{h_0^2\sigma}\Big)\frac{\beta}{\hat{h}^2}\hat{u}\hat{\zeta}.$$

We are given the following identities (Ianniello 1977):

$$\frac{U_0}{\sigma L_0} = \epsilon, \quad \frac{V_0}{\sigma D} = \epsilon, \quad \frac{g\zeta_0}{\sigma U_0 L_0} = 1,$$
$$\frac{h_0 U_0}{\sigma \zeta_0 L_0} = 1, \quad \text{and } \frac{h_0 V_0}{\sigma \zeta_0 D} = 1 \tag{3}$$

We also assign the following identity for notation: $\dfrac{\beta}{\sigma h_0} = \mathcal{D}$. Substituting (3) into the previous equation we have:

$$\frac{\partial \hat{u}}{\partial \hat{t}} + \epsilon\ \hat{u}\ \frac{\partial \hat{u}}{\partial \hat{x}} + \epsilon\ \hat{v}\ \frac{\partial \hat{u}}{\partial \hat{y}} = -\frac{\partial \hat{\zeta}}{\partial \hat{x}} - \mathcal{D}\frac{\hat{u}}{\hat{h}} + \mathcal{D}\epsilon\ \frac{\hat{u}\hat{\zeta}}{\hat{h}^2}.$$

We can now perform a perturbation analysis around a small parameter $\epsilon = \zeta_0/h$, which is a measure of the non-linearity of a system. It compares the tidal range to the undisturbed water depth. If the depth at low tide is sufficiently small compared with the tide, then friction throughout the water column will disproportionately effect flows during ebb tide, causing asymmetries in the tidal profile (aka non-linearities). The models used here rely on linear equations, thus this parameter needs to be assumed to be sufficiently small ($\epsilon = \zeta_0/h_0 << 1$). Using this method, we can isolate tidally forced terms from residuals.

When breaking these tidally dependent variables into constituent parts, the magnitude of each of these parts is assumed to be proportional to the non-linearity constant to varying degrees, ϵ. Thus, we express these as $\hat{u} = \hat{u_1} + \epsilon\hat{u_2} + \epsilon^2\hat{u_2}$+... similarly, for $\hat{v}$ and $\hat{\zeta}$ as presented in Li & Valle-Levinson 1999. Substituting these expanded terms, we then have:

$$\left[\frac{\partial \hat{u_1}}{\partial \hat{t}} + \epsilon \frac{\partial \hat{u_2}}{\partial \hat{t}} + ... \right] + \left[\epsilon \, \hat{u_1} \, \frac{\partial \hat{u_1}}{\partial \hat{x}} + \epsilon^2 \, \hat{u_1} \, \frac{\partial \hat{u_2}}{\partial \hat{x}} + \epsilon^2 \, \hat{u_2} \, \frac{\partial \hat{u_1}}{\partial \hat{x}} + ... \right] +$$
$$\left[\epsilon \, \hat{v_1} \, \frac{\partial \hat{u_1}}{\partial \hat{y}} + \epsilon^2 \, \hat{v_1} \, \frac{\partial \hat{u_2}}{\partial \hat{x}} + \epsilon^2 \, \hat{v_2} \, \frac{\partial \hat{u_1}}{\partial \hat{x}} + ... \right] = \left[- \frac{\partial \hat{\zeta_1}}{\partial \hat{x}} - \epsilon \, \frac{\partial \hat{\zeta_2}}{\partial \hat{x}} + ... \right] +$$
$$\left[\text{-D} \frac{\hat{u_1}}{\hat{h}} - \epsilon \, \mathcal{D} \frac{\hat{u_2}}{\hat{h}} + ... \right] + \left[\mathcal{D}\epsilon \, \frac{\hat{u_1}\hat{\zeta_1}}{\hat{h}^2} + \mathcal{D}\epsilon^2 \, \frac{\hat{u_1}\hat{\zeta_2}}{\hat{h}^2} + \mathcal{D}\epsilon^2 \, \frac{\hat{u_2}\hat{\zeta_1}}{\hat{h}^2} ... \right]$$

To obtain the first order $\mathcal{O}(1)$ tidally forced constituents, we eliminate higher order ($\mathcal{O}(\epsilon)$ etc.) terms. We then have:

$$\frac{\partial \hat{u_1}}{\partial \hat{t}} = -\frac{\partial \hat{\zeta_1}}{\partial \hat{x}} - \mathcal{D} \frac{\hat{u_1}}{\hat{h}} \tag{4}$$

We then return the variables to their dimensionalized forms by substituting the identities in (2) into equation (4):

$$\frac{\partial (u_1/U_0)}{\partial (t\sigma)} = -\frac{\partial (\zeta_1/\zeta_0)}{\partial (x/L_0)} - \mathcal{D} \frac{(u_1/U_0)}{(h/h_0)}$$

$$\frac{1}{\sigma U_0} \, \frac{\partial u_1}{\partial t} = -\frac{L_0}{\zeta_0} \, \frac{\partial \zeta_1}{\partial x} - \frac{h_0}{U_0} \mathcal{D} \frac{u_1}{h}$$

$$\sqrt{\frac{h_0}{g}} \frac{1}{\sigma \zeta_0} \, \frac{\partial u_1}{\partial t} = -\sqrt{\frac{g}{h_0}} \frac{\lambda/2\pi}{\zeta_0} \, \frac{\partial \zeta_1}{\partial x} - \frac{h_0}{\zeta_0} \sqrt{\frac{h_0}{g}} \mathcal{D} \frac{u_1}{h}$$

Dividing out the coefficient of the first term and rearranging, we are left with the following.

$$\frac{\partial u_1}{\partial t} = -g \frac{\partial \zeta_1}{\partial x} - \beta \frac{u_1}{h} \tag{5}$$

We will now follow a similar procedure using the second equation in (1):

$$\frac{\partial v}{\partial t} + u \frac{\partial v}{\partial x} + v \frac{\partial v}{\partial y} = -g \frac{\partial \zeta}{\partial y} - \beta \frac{v}{h} + \frac{\beta}{h^2} v\zeta.$$

We then non-dimensionalize using the identities in (2).

$$\frac{\partial(\hat{v}V_0)}{\partial(\hat{t}^1/_\sigma)} + (\hat{u}U_0)\frac{\partial(\hat{v}V_0)}{\partial(\hat{x}L_0)} + (\hat{v}V_0)\frac{\partial(\hat{v}V_0)}{\partial(\hat{y}D)} = -g\frac{\partial(\hat{\zeta}\zeta_0)}{\partial(\hat{y}D)} - \beta\frac{(\hat{v}V_0)}{(\hat{h}h_0)} + \frac{\beta}{(\hat{h}h_0)^2}(\hat{v}V_0)(\hat{\zeta}\zeta_0)$$

$$\left(V_0\ \sigma\right)\frac{\partial\hat{v}}{\partial\hat{t}} + \left(\frac{U_0V_0}{L_0}\right)\ \hat{u}\frac{\partial\hat{v}}{\partial\hat{x}} + \left(\frac{V_0^2}{D}\right)\ \hat{v}\frac{\partial\hat{v}}{\partial\hat{y}} = -\left(\frac{\zeta_0}{D}\right)g\frac{\partial\hat{\zeta}}{\partial\hat{y}}\ - \left(\frac{V_0}{h_0}\right)\beta\frac{\hat{v}}{\hat{h}} + \left(\frac{V_0\zeta_0}{h_0^2}\right)\frac{\beta}{\hat{h}^2}\hat{v}\hat{\zeta}$$

$$\frac{\partial\hat{v}}{\partial\hat{t}} + \left(\frac{U_0}{L_0\sigma}\right)\ \hat{u}\frac{\partial\hat{v}}{\partial\hat{x}} + \left(\frac{V_0}{D\sigma}\right)\ \hat{v}\frac{\partial\hat{v}}{\partial\hat{y}} = -\left(\frac{\zeta_0}{DV_0\sigma}\right)g\frac{\partial\hat{\zeta}}{\partial\hat{y}}\ - \left(\frac{1}{h_0\sigma}\right)\beta\frac{\hat{v}}{\hat{h}} + \left(\frac{\zeta_0}{h_0^2\sigma}\right)\frac{\beta}{\hat{h}^2}\hat{v}\hat{\zeta}$$

Expanding using identities (3), we know that $\frac{U_0}{L_0\sigma} = \epsilon$, and $\frac{V_0}{D\sigma} = \epsilon$. We also assign $\mathcal{D} = \frac{\beta}{h_0\sigma}$ and $\mathcal{H} = \frac{g\zeta_0}{DV_0\sigma}$.

$$\frac{\partial\hat{v}}{\partial\hat{t}} + \epsilon\ \hat{u}\frac{\partial\hat{v}}{\partial\hat{x}} + \epsilon\ \hat{v}\frac{\partial\hat{v}}{\partial\hat{y}} = \ -\mathcal{H}\frac{\partial\hat{\zeta}}{\partial\hat{y}} - \mathcal{D}\frac{\hat{v}}{\hat{h}} + \epsilon\ \mathcal{D}\frac{\beta}{\hat{h}^2}\hat{v}\hat{\zeta}$$

We will now perform a perturbation analysis, substituting $\hat{u} = \hat{u_1} + \epsilon\hat{u_2} + ...$ and similar for $\hat{v}$ and $\hat{\zeta}$.

$$\left[\ \frac{\partial\hat{v_1}}{\partial\hat{t}} + \epsilon\frac{\partial\hat{v_2}}{\partial\hat{t}} + ...\ \right]\ +\ \left[\ \epsilon\ \hat{u_1}\ \frac{\partial\hat{v_1}}{\partial\hat{x}} + \epsilon^2\ \hat{u_2}\ \frac{\partial\hat{v_1}}{\partial\hat{x}} + \epsilon^2\ \hat{u_1}\ \frac{\partial\hat{v_2}}{\partial\hat{x}} + ...\ \right]\ +$$
$$\left[\ \epsilon\ \hat{v_1}\ \frac{\partial\hat{v_1}}{\partial\hat{y}} + \epsilon^2\ \hat{v_2}\ \frac{\partial\hat{v_1}}{\partial\hat{y}} + \epsilon^2\ \hat{v_1}\ \frac{\partial\hat{v_2}}{\partial\hat{y}} + ...\ \right]\ =\ \left[-\ \mathcal{H}\ \frac{\partial\hat{\zeta_1}}{\partial\hat{y}} - \epsilon\ \mathcal{H}\ \frac{\partial\hat{\zeta_2}}{\partial\hat{y}} + ...\ \right]\ +$$
$$\left[\ \text{-D}\frac{\hat{v_1}}{\hat{h}} - \epsilon\ \mathcal{D}\frac{\hat{v_2}}{\hat{h}} + ...\ \ \right]\ +\ \left[\ \mathcal{D}\epsilon\ \frac{\hat{v_1}\hat{\zeta_1}}{\hat{h}^2} + \mathcal{D}\epsilon^2\ \frac{\hat{v_2}\hat{\zeta_1}}{\hat{h}^2} + \mathcal{D}\epsilon^2\ \frac{\hat{v_1}\hat{\zeta_2}}{\hat{h}^2} + ...\ \right]$$

We now select first order terms, $\mathcal{O}(1)$, and omit all others.

$$\frac{\partial\hat{v_1}}{\partial\hat{t}} = -\mathcal{H}\frac{\partial\hat{\zeta_1}}{\partial\hat{y}} - \mathcal{D}\frac{\hat{v_1}}{\hat{h}} \tag{6}$$

We then redimensionalize by substituting (2) into (6).

$$\frac{\partial\left(v_1/V_0\right)}{\partial\left(t\sigma\right)} = -\mathcal{H}\frac{\partial\left(\zeta_1/\zeta_0\right)}{\partial\left(y/D\right)} - \mathcal{D}\frac{\left(v_1/V_0\right)}{\left(h/h_0\right)}$$

$$\Big(\frac{1}{V_0\sigma}\Big)\frac{\partial v_1}{\partial t} = -\Big(\frac{D}{\zeta_0}\Big)\mathcal{H}\frac{\partial \zeta_1}{\partial y} - \Big(\frac{h_0}{V_0}\Big)\mathcal{D}\frac{v_1}{h}$$

$$\frac{\partial v_1}{\partial t} = -\Big(\frac{DV_0\sigma}{\zeta_0}\Big)\mathcal{H}\frac{\partial \zeta_1}{\partial y} - \Big(h_0\sigma\Big)\mathcal{D}\frac{v_1}{h}$$

$$\frac{\partial v_1}{\partial t} = -\Big(\frac{DV_0\sigma}{\zeta_0}\Big)\Big(\frac{g\zeta_0}{DV_0\sigma}\Big)\frac{\partial \zeta_1}{\partial y} - \Big(h_0\sigma\Big)\mathcal{D}\frac{v_1}{h}$$

$$\frac{\partial v_1}{\partial t} = -g\frac{\partial \zeta_1}{\partial y} - \beta\frac{v_1}{h} \tag{7}$$

What remains is a non-homogenous first order linear differential equation.

We will now follow the same procedure to isolate the first order terms for the third equation in the Navier-Stokes equations.

$$\frac{\partial \zeta}{\partial t} + \frac{\partial (h+\zeta)u}{\partial x} + \frac{\partial (h+\zeta)v}{\partial y} = 0$$

Substituting various identities from (2) into this equation gives us the following.

$$\frac{\partial\big(\hat{\zeta}\zeta_0\big)}{\partial \hat{t}} + \frac{\partial\big((\hat{h}h_0) + (\hat{\zeta}\zeta_0)\big)(\hat{u}U_0)}{\partial(\hat{x}L_0)} + \frac{\partial\big((\hat{h}h_0) + (\hat{\zeta}\zeta_0)\big)(\hat{v}V_0)}{\partial(\hat{y}D)} = 0$$

$$\Big(\zeta_0\sigma\Big)\frac{\partial \hat{\zeta}}{\partial \hat{t}} + \Big(\frac{U_0}{L_0}\Big)\frac{\partial\big(\hat{h}h_0 + \hat{\zeta}\zeta_0\big)\hat{u}}{\partial \hat{x}} + \Big(\frac{V_0}{D}\Big)\frac{\partial\big(\hat{h}h_0 + \hat{\zeta}\zeta_0\big)\hat{v}}{\partial \hat{y}} = 0$$

$$\Big(\zeta_0\sigma\Big)\frac{\partial \hat{\zeta}}{\partial \hat{t}} + \Big(\frac{U_0h_0}{L_0}\Big)\frac{\partial\big(\hat{h} + \epsilon\hat{\zeta}\big)\hat{u}}{\partial \hat{x}} + \Big(\frac{V_0h_0}{D}\Big)\frac{\partial\big(\hat{h} + \epsilon\hat{\zeta}\big)\hat{v}}{\partial \hat{y}} = 0$$

$$\frac{\partial \hat{\zeta}}{\partial \hat{t}} + \Big(\frac{U_0h_0}{L_0\zeta_0\sigma}\Big)\frac{\partial\big(\hat{h} + \epsilon\hat{\zeta}\big)\hat{u}}{\partial \hat{x}} + \Big(\frac{V_0h_0}{D\zeta_0\sigma}\Big)\frac{\partial\big(\hat{h} + \epsilon\hat{\zeta}\big)\hat{v}}{\partial \hat{y}} = 0$$

We also know from (3) that $\frac{U_0h_0}{L_0\zeta_0\sigma} = 1$ and $\frac{V_0h_0}{D\zeta_0\sigma} = 1$.

$$\frac{\partial \hat{\zeta}}{\partial \hat{t}} + \frac{\partial\big(\hat{h} + \epsilon\hat{\zeta}\big)\hat{u}}{\partial \hat{x}} + \frac{\partial\big(\hat{h} + \epsilon\hat{\zeta}\big)\hat{v}}{\partial \hat{y}} = 0$$

$$\frac{\partial \hat{\zeta}}{\partial \hat{t}} + \frac{\partial \hat{h}\hat{u}}{\partial \hat{x}} + \epsilon \frac{\partial \hat{\zeta}\hat{u}}{\partial \hat{x}} + \frac{\partial \hat{h}\hat{v}}{\partial \hat{y}} + \epsilon \frac{\partial \hat{\zeta}\hat{v}}{\partial \hat{y}} = 0$$

We now perform a perturbation analysis by substituting $\hat{u} = \hat{u_1} + \epsilon\hat{u_2} + \epsilon^2\hat{u_3} + ...$ (similarly for $\hat{v}$ and $\hat{\zeta}$).

$$\left[\frac{\partial \hat{\zeta_1}}{\partial \hat{t}} + \epsilon \frac{\partial \hat{\zeta_2}}{\partial \hat{t}} + ... \right] + \left[\frac{\partial \hat{h}\hat{u_1}}{\partial \hat{x}} + \epsilon \frac{\partial \hat{h}\hat{u_2}}{\partial \hat{x}} + ... \right] + \left[\epsilon \frac{\partial \hat{\zeta_1}\hat{u_1}}{\partial \hat{x}} + \epsilon^2 \frac{\partial \hat{\zeta_1}\hat{u_2}}{\partial \hat{x}} + \epsilon^2 \frac{\partial \hat{\zeta_2}\hat{u_1}}{\partial \hat{x}} + ... \right]$$
$$+ \left[\frac{\partial \hat{h}\hat{v_1}}{\partial \hat{y}} + \epsilon \frac{\partial \hat{h}\hat{v_2}}{\partial \hat{y}} + ... \right] + \left[\epsilon \frac{\partial \hat{\zeta_1}\hat{v_1}}{\partial \hat{y}} + \epsilon^2 \frac{\partial \hat{\zeta_1}\hat{v_2}}{\partial \hat{y}} + \epsilon^2 \frac{\partial \hat{\zeta_2}\hat{v_1}}{\partial \hat{y}} + ... \right] = 0$$

We now select all terms of $\mathcal{O}(1)$ (order 1).

$$\frac{\partial \hat{\zeta_1}}{\partial \hat{t}} + \frac{\partial \hat{h}\hat{u_1}}{\partial \hat{x}} + \frac{\partial \hat{h}\hat{v_1}}{\partial \hat{y}} = 0 \tag{8}$$

We can now substitute identities from (2) into (8) to redimensionalize.

$$\frac{\partial (\zeta_1/\zeta_0)}{\partial (t\sigma)} + \frac{\partial (h/h_0)(u_1/U_0)}{\partial (x/L_0)} + \frac{\partial (h/h_0)(v_1/V_0)}{\partial (y/D)} = 0$$

$$\left(\frac{1}{\zeta_0 \sigma}\right)\frac{\partial \zeta_1}{\partial t} + \left(\frac{L_0}{h_0 U_0}\right)\frac{\partial h u_1}{\partial x} + \left(\frac{D}{h_0 V_0}\right)\frac{\partial h v_1}{\partial y} = 0$$

$$\frac{\partial \zeta_1}{\partial t} + \left(\frac{L_0 \zeta_0 \sigma}{h_0 U_0}\right)\frac{\partial h u_1}{\partial x} + \left(\frac{D \zeta_0 \sigma}{h_0 V_0}\right)\frac{\partial h v_1}{\partial y} = 0$$

$$\frac{\partial \zeta_1}{\partial t} + h\frac{\partial u_1}{\partial x} + \frac{\partial h v_1}{\partial y} = 0 \tag{9}$$

We now have three differential equations representing the behavior or the first order tidally forced variables.

$$\frac{\partial u_1}{\partial t} = -g\frac{\partial \zeta_1}{\partial x} - \beta\frac{u_1}{h}$$
$$\frac{\partial v_1}{\partial t} = -g\frac{\partial \zeta_1}{\partial y} - \beta\frac{v_1}{h}$$
$$\frac{\partial \zeta_1}{\partial t} + h\frac{\partial u_1}{\partial x} + \frac{\partial h v_1}{\partial y} = 0 \tag{10}$$

The solutions to these differential equations, for a single-frequency tide, can be expressed as follows, as we are applying a tidal wave to the domain (as presented in Li & Valle-Levinson, 1999):

$$u_1 = Ue^{i\sigma t}, \quad v_1 = Ve^{i\sigma t}, \text{ and } \zeta_1 = Ae^{i\sigma t} \tag{11}$$

Substituting (11) into the first equation in (10) gives:

$$\frac{\partial Ue^{i\sigma t}}{\partial t} = -g\frac{\partial Ae^{i\sigma t}}{\partial \hat{x}} - \mathcal{D}\frac{Ue^{i\sigma t}}{\hat{h}}$$
$$Ui\sigma e^{i\sigma t} = -ge^{i\sigma t}\frac{\partial A}{\partial x} - \frac{\beta U e^{i\sigma t}}{\sigma h_0 \hat{h}}$$
$$U = \frac{-g}{i\sigma + {}^{\beta}/_{h}}(\frac{\partial A}{\partial x}) \tag{12}$$

We must then solve for A. In this process, we assume that the lateral variation in A is negligible (or that $\frac{\partial A}{\partial y} = 0$) as presented in Li & Valle-Levinson, 1999.
Substituting (11) into (9) gives us a useful relationship.

$$\frac{\partial Ae^{i\sigma t}}{\partial t} + h\frac{\partial Ue^{i\sigma t}}{\partial x} + \frac{\partial hVe^{i\sigma t}}{\partial y} = 0$$

$$Ai\sigma e^{i\sigma t} + he^{i\sigma t}\frac{\partial U}{\partial x} + e^{i\sigma t}\frac{\partial hV}{\partial y} = 0$$

$$Ai\sigma + h\frac{\partial U}{\partial x} + \frac{\partial hV}{\partial y} = 0$$

Multiplying through by h, and then taking the lateral integral over the width of the estuary yields the following.

$$\int_0^D i\sigma A dy + \int_0^D h\frac{\partial U}{\partial x}dy + \int_0^D \frac{\partial hV}{\partial y}dy = 0$$

$$i\sigma Ay \Big|_0^D + \int_0^D h\frac{\partial U}{\partial x}dy + \Big|_0^D hV = 0$$

Applying boundary conditions: $A\Big|_{x=0} = \zeta_0$, $\frac{\partial A}{\partial x}\Big|_{x=L} = 0$, and $V\Big|_{y=0,D} = 0$.

$$i\sigma AD + \int_0^D h\frac{\partial U}{\partial x}dy = 0$$

Now we consider $\int_0^D h\frac{\partial U}{\partial x}dy$. Taking our equation (12), multiplying by h and taking the derivative over x.

$$U = \frac{-g}{i\sigma + {}^{\beta}/_{h}}(\frac{\partial A}{\partial x})$$

$$\frac{\partial Uh}{\partial x} = \frac{\partial}{\partial x}\Big(\frac{-gh}{i\sigma + {}^{\beta}/_{h}}(\frac{\partial A}{\partial x})\Big)$$

We know that $h,\ g,\ i,\ \sigma$, and β are independent of x, giving

$$h\ \frac{\partial U}{\partial x} = \frac{-gh}{i\sigma + {}^{\beta}/_{h}}(\frac{\partial^2 A}{\partial x^2})$$

We then integrate over the width of the channel.

$$\int_0^D h\ \frac{\partial U}{\partial x}dy = \int_0^D \frac{-gh}{i\sigma + {}^{\beta}/_{h}}(\frac{\partial^2 A}{\partial x^2})dy$$

Because we are assuming that the lateral variation in water level amplitude is negligible, we can pull the second derivative out of the integral. We also assign the following identity: $\mathcal{F} = \int_0^D \frac{-gh}{i\sigma + {}^{\beta}/_{h}}dy$, which is a constant.

$$\int_0^D h\ \frac{\partial U}{\partial x}dy = \mathcal{F}(\frac{\partial^2 A}{\partial x^2})$$

Plugging this in, we are then left with the following second order, homogenous, constant coefficient differential equation:

$$i\sigma AD + \int_0^D h\frac{\partial U}{\partial x}dy = 0,$$
$$i\sigma AD + F\frac{\partial^2 A}{\partial x^2} = 0.$$

This has the following characteristic equation.

With roots

$$Fr^2 + 0r + Di\sigma = 0$$
$$r_1 = \sqrt{\frac{-Di\sigma}{F}} \quad \text{and} \quad r_2 = -\sqrt{\frac{-Di\sigma}{F}}.$$

These are complex roots, thus we have the following general solution form:

$$A(x) = exp\Big(\frac{-bx}{2a}\Big)\Big[c_1\cos(\beta_1 x) + c_2\sin(\beta_1 x)\Big]$$

With $a = \mathcal{F}$, $b = 0$, $c = Di\sigma$, and

$$\beta_1 = \frac{\sqrt{4ac - b^2}}{2a} = \frac{\sqrt{4\mathcal{F}i\sigma D}}{2\mathcal{F}} = \sqrt{\frac{i\sigma D}{\mathcal{F}}} = \omega.$$

Plugging these in we have

$$A(x) = exp(0)\Big[c_1\cos(\omega x) + c_2\sin(\omega x)\Big] = c_1\cos(\omega x) + c_2\sin(\omega x).$$

We then apply the following boundary conditions to solve for c_1 and c_2,

$$A\mid_{x=0} = \zeta_0, \text{ and } \frac{\partial A}{\partial x}\mid_{x=L} = 0.$$

For c_1,

$$A(0) = c_1\cos(0) + c_2\sin(0) = \zeta_0 = c_1.$$

Thus,

$$A(x) = \zeta_0\cos(\omega x) + c_2\sin(\omega x).$$

Taking the derivative, we evaluate at $x = L$ to use our second boundary condition.

$$A'(x) = -\zeta_0\ \omega \sin(\omega x) + c_2 \cos(\omega x)$$

$$A'(L) = -\zeta_0\ \omega \sin(\omega L) + c_2 \cos(\omega L) = 0$$

$$c_2 \cos(\omega L) = \zeta_0\ \omega \sin(\omega L)$$

$$c_2 = \zeta_0 \frac{\sin(\omega L)}{\cos(\omega L)} = \zeta_0 \tan(\omega L)$$

Thus, we have

$$\begin{aligned}
A &= \zeta_0 \cos(\omega x) + \zeta_0 \tan(\omega L) \sin(\omega x) \\
&= \zeta_0 \Big[\frac{\cos(\omega x)\cos(\omega L)}{\cos(\omega L)} + \frac{\sin(\omega L)\sin(\omega x)}{\cos(\omega L)} \Big] \\
&= \zeta_0 \Big[\frac{\cos(\omega x)\cos(\omega L) + \sin(\omega L)\sin(\omega x)}{\cos(\omega L)} \Big] \\
&= \zeta_0 \Big[\frac{\cos(\omega x - \omega L)}{\cos(\omega L)} \Big] * \\
&= \zeta_0 \frac{\cos[\omega(x - L)]}{\cos(\omega L)}.
\end{aligned}$$

$$*\cos(\alpha - \beta) = \cos(\alpha)\cos(\beta) + \sin(\alpha)\sin(\beta)$$

The complex coefficients of axial velocity, across channel velocity, and water level elevation respectively are therefore

$$U = \frac{-g}{i\sigma + \beta/h} \Big(\frac{\partial A}{\partial x} \Big)$$

$$\frac{\partial A}{\partial x} = -\zeta_0\ \omega \frac{\sin(\omega x - \omega L)}{\cos(\omega L)}$$

$$U = \frac{g \zeta_0 \omega}{(i\sigma + \beta/h)} \frac{\sin(\omega x - \omega L)}{\cos(\omega L)}\ .$$

with

$$\omega = \sqrt{\frac{i\sigma D}{F}}, \quad \text{and} \quad F = -\int_0^D \frac{gh}{i\sigma + \beta/h} dy.$$

Now, we substitute the assigned single-frequency tide using $u_1 = Ue^{i\sigma t}$, $v_1 = Ve^{i\sigma t}$, and $\zeta_1 = Ae^{i\sigma t}$.

$$\frac{\partial Ae^{i\sigma t}}{\partial t} + h\frac{\partial Ue^{i\sigma t}}{\partial x} + \frac{\partial hVe^{i\sigma t}}{\partial y} = 0$$

$$Ai\sigma e^{i\sigma t} + he^{i\sigma t}\frac{\partial U}{\partial x} + e^{i\sigma t}\frac{\partial hV}{\partial y} = 0$$

$$Ai\sigma + h\frac{\partial U}{\partial x} + \frac{\partial hV}{\partial y} = 0$$

We know from earlier that

$$\begin{aligned}\frac{\partial U}{\partial x} &= \frac{\partial}{\partial x}\Big[\Big(\frac{g\zeta_0\omega}{(i\sigma + {}^{\beta}/_{h})}\Big)\Big(\frac{\sin(\omega x - \omega L)}{\cos(\omega L)}\Big)\Big] \\ &= \Big(\frac{g\zeta_0\omega}{(i\sigma + {}^{\beta}/_{h})}\Big)\Big(\frac{\omega\cos(\omega x - \omega L)}{\cos(\omega L)}\Big) \\ &= A\frac{g\omega^2}{i\sigma + {}^{\beta}/_{h}}.\end{aligned}$$

Thus,

$$Ai\sigma + hA\frac{g\omega^2}{i\sigma + {}^{\beta}/_{h}} + \frac{\partial hV}{\partial y} = 0.$$

We then integrate across the estuary.

$$\int_0^y Ai\sigma dy + \int_0^y hA\frac{g\omega^2}{i\sigma + {}^{\beta}/_{h}}dy + \int_0^y \frac{\partial hV}{\partial y}dy = 0$$

$$Ai\sigma y\Big|_0^y + hA\int_0^y \frac{g\omega^2}{i\sigma + {}^{\beta}/_{h}}dy + hV\Big|_0^y = 0$$

$$Ai\sigma y + hA\int_0^y \frac{g\omega^2}{i\sigma + {}^{\beta}/_{h}}dy + hV = 0$$

Rearranging, we have

$$V = \frac{-A}{h}\Big[i\sigma y + \int_0^D \frac{gh\omega^2}{i\sigma + {}^{\beta}/_{h}}\Big] .$$

The resulting first order equations describing tidally forced flow and water level are as follows:

$$u_1 = Ue^{i\sigma t}, \quad v_1 = Ve^{i\sigma t}, \text{ and } \zeta_1 = Ae^{i\sigma t}$$

with

$$U = \frac{g\zeta_0\omega}{(i\sigma + {}^{\beta}/_{h})} \frac{\sin(\omega x - \omega L)}{\cos(\omega L)} \ ,$$

$$A = \zeta_0 \frac{\cos[\omega(x-L)]}{\cos(\omega L)} \ ,$$

$$V = \frac{-A}{h}\Big[i\sigma y + \int_0^D \frac{gh\omega^2}{i\sigma + {}^{\beta}/_{h}}\Big] \ ,$$

$$\omega = \sqrt{\frac{i\sigma D}{F}}, \quad \text{and} \quad F = -\int_0^D \frac{gh}{i\sigma + {}^{\beta}/_{h}} dy.$$

3.2 Second Order Equations

We begin again with the perturbation expansion of the non-dimensionalized shallow water Navier Stokes equations for axial velocity from earlier:

$$\Big[\ \frac{\partial \hat{u_1}}{\partial \hat{t}} + \epsilon \frac{\partial \hat{u_2}}{\partial \hat{t}} + ...\ \Big] \ + \ \Big[\ \epsilon\ \hat{u_1}\ \frac{\partial \hat{u_1}}{\partial \hat{x}} + \epsilon^2\ \hat{u_1}\ \frac{\partial \hat{u_2}}{\partial \hat{x}} + \epsilon^2\ \hat{u_2}\ \frac{\partial \hat{u_1}}{\partial \hat{x}} + ...\ \Big] \ +$$
$$\Big[\ \epsilon\ \hat{v_1}\ \frac{\partial \hat{u_1}}{\partial \hat{y}} + \epsilon^2\ \hat{v_1}\ \frac{\partial \hat{u_2}}{\partial \hat{x}} + \epsilon^2\ \hat{v_2}\ \frac{\partial \hat{u_1}}{\partial \hat{x}} + ...\ \Big] \ = \ \Big[\ -\frac{\partial \hat{\zeta_1}}{\partial \hat{x}} - \epsilon\ \frac{\partial \hat{\zeta_2}}{\partial \hat{x}} + ...\ \Big] \ +$$
$$\Big[\ \text{-D}\frac{\hat{u_1}}{\hat{h}} - \epsilon\ \mathcal{D}\frac{\hat{u_2}}{\hat{h}} + ...\ \Big] \ + \ \Big[\ \mathcal{D}\epsilon\ \frac{\hat{u_1}\hat{\zeta_1}}{\hat{h}^2} + \mathcal{D}\epsilon^2\ \frac{\hat{u_1}\hat{\zeta_2}}{\hat{h}^2} + \mathcal{D}\epsilon^2\ \frac{\hat{u_2}\hat{\zeta_1}}{\hat{h}^2} ...\ \Big]$$

We now select the $\mathcal{O}(\epsilon)$ terms, eliminating higher terms and $\mathcal{O}(1)$. This gives us:

$$\frac{\partial \hat{u_2}}{\partial t} + \hat{u_1}\frac{\partial \hat{u_1}}{\partial \hat{x}} + \hat{v_1}\frac{\partial \hat{u_1}}{\partial \hat{y}} = -\frac{\partial \hat{\zeta_2}}{\partial \hat{x}} - \mathcal{D}\frac{\hat{u_2}}{\hat{h}} + \mathcal{D}\frac{\hat{u_1}\hat{\zeta_1}}{\hat{h^2}}$$

Returning to dimensionalized variables, using previous identities:

$$\frac{\partial\big({}^{u_2}/_{U_0}\big)}{\partial(\sigma t)} + \Big(\frac{u_1}{U_0}\Big)\frac{\partial\big({}^{u_1}/_{U_0}\big)}{\partial\big({}^{x}/_{L_0}\big)} + \Big(\frac{v_1}{V_0}\Big)\frac{\partial\big({}^{u_1}/_{U_0}\big)}{\partial\big({}^{y}/_{D}\big)} = -\frac{\partial\big({}^{\zeta_2}/_{\zeta_0}\big)}{\partial\big({}^{x}/_{L_0}\big)} - \mathcal{D}\frac{\big({}^{u_2}/_{U_0}\big)}{\big({}^{h}/_{h_0}\big)} + \mathcal{D}\frac{\big({}^{u_1}/_{U_0}\big)\big({}^{\zeta_1}/_{\zeta_0}\big)}{\big({}^{h^2}/_{h_0^2}\big)}$$

$$\Big(\frac{1}{U_0\sigma}\Big)\frac{\partial u_2}{\partial t}+\Big(\frac{L_0}{U_0^2}\Big)u_1\frac{\partial u_1}{\partial x}+\Big(\frac{D}{U_0V_0}\Big)v_1\frac{\partial u_1}{\partial y}=-\Big(\frac{L_0}{\zeta_0}\Big)\frac{\partial \zeta_0}{\partial x}-\Big(\frac{h_0}{U_0}\Big)\mathcal{D}\frac{u_2}{h}+\Big(\frac{h_0^2}{U_0\zeta_0}\Big)\mathcal{D}\frac{u_1\zeta_1}{h^2}$$

We then take the tidal average (through time), noting that the coefficients are constant, and h is not a function of t. This also eliminates the first term, which is a time dependent derivative.

$$\Big(\frac{L_0}{U_0^2}\Big)\overline{u_1\frac{\partial u_1}{\partial x}}+\Big(\frac{D}{U_0V_0}\Big)\overline{v_1\frac{\partial u_1}{\partial y}}=-\Big(\frac{L_0}{\zeta_0}\Big)\frac{\partial\overline{\zeta_0}}{\partial x}-\Big(\frac{h_0}{U_0}\Big)\mathcal{D}\frac{\overline{u_2}}{h}+\Big(\frac{h_0^2}{U_0\zeta_0}\Big)\mathcal{D}\frac{\overline{u_1\zeta_1}}{h^2}$$

We then eliminate the coefficient on the first term by multiplying through by $\dfrac{U_0^2}{L_0}$.

$$\overline{u_1\frac{\partial u_1}{\partial x}}+\Big(\frac{U_0D}{L_0V_0}\Big)\overline{v_1\frac{\partial u_1}{\partial y}}=-\Big(\frac{U_0^2}{\zeta_0}\Big)\frac{\partial\overline{\zeta_0}}{\partial x}-\Big(\frac{U_0h_0}{L_0}\Big)\mathcal{D}\frac{\overline{u_2}}{h}+\Big(\frac{U_0h_0^2}{L_0\zeta_0}\Big)\mathcal{D}\frac{\overline{u_1\zeta_1}}{h^2}$$

Using the identities given in Li & O'Donnell 2005, we can expand the coefficient terms:

$$U_0=\zeta_0\sqrt{g/h_0},\quad L_0=(\sqrt{gh_0})/\sigma,\quad\text{and}\quad V_0=(\zeta_0/h_0)\sigma D.$$

For conciseness we assign the following identities:

$$a=\overline{u_1\frac{\partial u_1}{\partial x}},\quad b=\overline{v_1\frac{\partial u_1}{\partial y}},\quad c=\frac{\partial\overline{\zeta_0}}{\partial x},\quad d=\frac{\overline{u_2}}{h},\quad\text{and}\quad e=\frac{\overline{u_1\zeta_1}}{h^2}.$$

$$a+\Big(\frac{(\zeta_0\sqrt{g/h_0})D}{((\sqrt{gh_0})/\sigma)(D(\zeta_0/h_0)\sigma)}\Big)b=-\Big(\frac{\zeta_0^2(g/h_0)}{\zeta_0}\Big)c-\Big(\frac{(\zeta_0\sqrt{g/h_0})h_0}{((\sqrt{gh_0})/\sigma)}\Big)\mathcal{D}d+\Big(\frac{(\zeta_0\sqrt{g/h_0})h_0^2}{((\sqrt{gh_0})/\sigma)\zeta_0}\Big)\mathcal{D}e$$

$$a+\Big(\frac{\zeta_0\sqrt{g}D\sigma h_0}{\sqrt{g}h_0D\zeta_0\sigma}\Big)b=-\Big(\frac{\zeta_0^2g}{\zeta_0h_0}\Big)c-\Big(\frac{\zeta_0\sqrt{g}h_0\sigma}{\sqrt{gh_0}\sqrt{h_0}}\Big)\mathcal{D}d+\Big(\frac{\zeta_0\sqrt{g}h_0^2\sigma}{\sqrt{gh_0}\zeta_0\sqrt{h_0}}\Big)\mathcal{D}e$$

$$a+b=-\Big(\frac{\zeta_0g}{h_0}\Big)c-\Big(\zeta_0\sigma\Big)\mathcal{D}d+\Big(h_0\sigma\Big)\mathcal{D}e$$

Expanding $\mathcal{D}=\beta/h_0\sigma$:

$$a+b=-\Big(\frac{\zeta_0 g}{h_0}\Big)c-\Big(\zeta_0\sigma\Big)\Big(\frac{\beta}{h_0\sigma}\Big)d+\Big(h_0\sigma\Big)\Big(\frac{\beta}{h_0\sigma}\Big)e$$

$$a+b=-\Big(\frac{\zeta_0}{h_0}\Big)g\ c-\Big(\frac{\zeta_0}{h_0}\Big)\beta d+\beta e$$

And $\epsilon=\frac{\zeta_0}{h_0}$. We are left with the following:

$$\overline{u_1\frac{\partial u_1}{\partial x}}+\overline{v_1\frac{\partial u_1}{\partial y}}=-\epsilon g\frac{\partial\overline{\zeta_2}}{\partial x}-\epsilon\beta\frac{\overline{u_2}}{h}+\beta\frac{\overline{u_1\zeta_1}}{h^2} \tag{13}$$

Rearranging the previous equation yields:

$$\overline{u_2}=\frac{\overline{\zeta_1 u_1}}{\epsilon h}+-\frac{h}{\epsilon\beta}\Big(\overline{u_1\frac{\partial u_1}{\partial x}}+\overline{v_1\frac{\partial u_1}{\partial y}}\Big)+-\frac{gh}{\beta}\frac{\partial\overline{\zeta_2}}{\partial x}$$

We now apply the following formula presented in Li, 1996:

$$u_T=\overline{u_2}+\frac{\overline{\zeta_1 u_1}}{h}+\text{ higher order terms.}$$

Thus, along channel transport is described by

$$u_T=\frac{\overline{\zeta_1 u_1}}{\epsilon h}+\frac{\overline{\zeta_1 u_1}}{h}+-\frac{h}{\beta}\Big(\overline{u_1\frac{\partial u_1}{\partial x}}+\overline{v_1\frac{\partial u_1}{\partial y}}\Big)+-\frac{gh}{\beta}\frac{\partial\overline{\zeta_2}}{\partial x} \tag{14}$$

We can follow a similar procedure to find v_2 and thus v_T. We begin with the perturbation expansion of the second equation in the Navier-Stokes equations:

$$\Big[\ \frac{\partial\hat{v_1}}{\partial\hat{t}}+\epsilon\frac{\partial\hat{v_2}}{\partial\hat{t}}+...\ \Big]\ +\ \Big[\ \epsilon\ \hat{u_1}\ \frac{\partial\hat{v_1}}{\partial\hat{x}}+\epsilon^2\ \hat{u_2}\ \frac{\partial\hat{v_1}}{\partial\hat{x}}+\epsilon^2\ \hat{u_1}\ \frac{\partial\hat{v_2}}{\partial\hat{x}}+...\ \Big]\ +$$
$$\Big[\ \epsilon\ \hat{v_1}\ \frac{\partial\hat{v_1}}{\partial\hat{y}}+\epsilon^2\ \hat{v_2}\ \frac{\partial\hat{v_1}}{\partial\hat{y}}+\epsilon^2\ \hat{v_1}\ \frac{\partial\hat{v_2}}{\partial\hat{y}}+...\ \Big]\ =\ \Big[-\ \mathcal{H}\ \frac{\partial\hat{\zeta_1}}{\partial\hat{y}}-\epsilon\ \mathcal{H}\ \frac{\partial\hat{\zeta_2}}{\partial\hat{y}}+...\ \Big]\ +$$
$$\Big[\ \text{-D}\frac{\hat{v_1}}{\hat{h}}-\epsilon\ \mathcal{D}\frac{\hat{v_2}}{\hat{h}}+...\quad\Big]\ +\ \Big[\ \mathcal{D}\epsilon\ \frac{\hat{v_1}\hat{\zeta_1}}{\hat{h}^2}+\mathcal{D}\epsilon^2\ \frac{\hat{v_2}\hat{\zeta_1}}{\hat{h}^2}+\mathcal{D}\epsilon^2\ \frac{\hat{v_1}\hat{\zeta_2}}{\hat{h}^2}+...\ \Big]$$

Terms of $\mathcal{O}(\epsilon)$ are then isolated.

$$\frac{\partial \hat{v_2}}{\partial t} + \hat{u_1}\frac{\partial \hat{v_1}}{\partial \hat{x}} + \hat{v_1}\frac{\partial \hat{v_1}}{\partial \hat{y}} = -\mathcal{H}\frac{\partial \hat{\zeta_2}}{\partial \hat{y}} - \mathcal{D}\frac{\hat{v_2}}{\hat{h}} + \mathcal{D}\frac{\hat{v_1}\hat{\zeta_1}}{\hat{h}^2}$$

We can redimensionalize using the similar procedures to those in isolating u_2.

$$\frac{\partial\left(v_2/V_0\right)}{\partial(\sigma t)} + \left(\frac{u_1}{U_0}\right)\frac{\partial\left(v_1/V_0\right)}{\partial\left(x/L_0\right)} + \left(\frac{v_1}{V_0}\right)\frac{\partial\left(v_1/V_0\right)}{\partial\left(y/D\right)} = -\mathcal{H}\frac{\partial\left(\zeta_2/\zeta_0\right)}{\partial\left(y/D\right)} - \mathcal{D}\frac{\left(v_2/V_0\right)}{\left(h/h_0\right)} + \mathcal{D}\frac{\left(v_1/V_0\right)\left(\zeta_1/\zeta_0\right)}{\left(h^2/h_0^2\right)}$$

Rearranging,

$$\overline{u_1\frac{\partial v_1}{\partial x}} + \overline{v_1\frac{\partial v_1}{\partial y}} = -\epsilon g\frac{\partial \overline{\zeta_2}}{\partial y} - \epsilon\beta\frac{\overline{v_2}}{h} + \beta\frac{\overline{v_1\zeta_1}}{h^2}\ . \tag{15}$$

$$v_2 = \frac{\overline{\zeta_1 v_1}}{\epsilon h} + -\frac{h}{\epsilon\beta}\left(\overline{u_1\frac{\partial v_1}{\partial x}} + \overline{v_1\frac{\partial v_1}{\partial y}}\right) + -\frac{gh}{\beta}\frac{\partial\overline{\zeta_2}}{\partial y}$$

The transport velocity (v_T) can be obtained using the equation presented in Li, 1996:

$$v_T = \overline{v_2} + \frac{\overline{\zeta_1 v_1}}{h} + \text{ higher order terms.}$$

Thus,

$$v_T = \frac{\overline{\zeta_1 v_1}}{\epsilon h} + \frac{\overline{\zeta_1 v_1}}{h} + -\frac{h}{\beta}\left(\overline{u_1\frac{\partial v_1}{\partial x}} + \overline{v_1\frac{\partial v_1}{\partial y}}\right) + -\frac{gh}{\beta}\frac{\partial\overline{\zeta_2}}{\partial y}$$

The final second order equation begins with the expansion used to derive the equation for ζ_1:

$$\left[\ \frac{\partial\hat{\zeta_1}}{\partial\hat{t}} + \epsilon\frac{\partial\hat{\zeta_2}}{\partial\hat{t}} + \ldots\ \right] + \left[\ \frac{\partial\hat{h}\hat{u_1}}{\partial\hat{x}} + \epsilon\ \frac{\partial\hat{h}\hat{u_2}}{\partial\hat{x}} + \ldots\ \right] + \left[\ \epsilon\ \frac{\partial\hat{\zeta_1}\hat{u_1}}{\partial\hat{x}} + \epsilon^2\ \frac{\partial\hat{\zeta_1}\hat{u_2}}{\partial\hat{x}} + \epsilon^2\ \frac{\partial\hat{\zeta_2}\hat{u_1}}{\partial\hat{x}} + \ldots\ \right]$$
$$+ \left[\ \frac{\partial\hat{h}\hat{v_1}}{\partial\hat{y}} + \epsilon\ \frac{\partial\hat{h}\hat{v_2}}{\partial\hat{y}} + \ldots\ \right] + \left[\ \epsilon\ \frac{\partial\hat{\zeta_1}\hat{v_1}}{\partial\hat{y}} + \epsilon^2\ \frac{\partial\hat{\zeta_1}\hat{v_2}}{\partial\hat{y}} + \epsilon^2\ \frac{\partial\hat{\zeta_2}\hat{v_1}}{\partial\hat{y}} + \ldots\ \right] = 0$$

Selecting all terms $\mathcal{O}(\epsilon)$ yields

$$\frac{\partial\hat{\zeta_2}}{\partial\hat{t}} + \frac{\partial\hat{h}\hat{u_2}}{\partial\hat{x}} + \frac{\partial\hat{\zeta_1}\hat{u_1}}{\partial\hat{x}} + \frac{\partial\hat{h}\hat{v_2}}{\partial\hat{y}} + \frac{\partial\hat{\zeta_1}\hat{v_1}}{\partial\hat{y}} = 0$$

Taking the tidal average yields the following.

$$\frac{\partial \hat{h}\overline{\hat{u_2}}}{\partial \hat{x}} + \frac{\partial \overline{\hat{\zeta_1}\hat{u_1}}}{\partial \hat{x}} + \frac{\partial \overline{\hat{h}\hat{v_2}}}{\partial \hat{y}} + \frac{\partial \overline{\hat{\zeta_1}\hat{v_1}}}{\partial \hat{y}} = 0$$

Then, substitute identities from (2) to redimensionalize.

$$h\frac{\partial \overline{u_2}}{\partial x} + \frac{\partial \overline{\zeta_1 u_1}}{\partial x} + \frac{\partial \overline{h v_2}}{\partial y} + \frac{\partial \overline{\zeta_1 v_1}}{\partial y} = 0$$

However, it has been established that

$$u_T = \overline{u_2} + \frac{\overline{\zeta_1 u_1}}{h} + \text{ higher order terms}$$

and

$$v_T = \overline{v_2} + \frac{\overline{\zeta_1 v_1}}{h} + \text{ higher order terms.}$$

Thus,

$$h\frac{\partial u_T}{\partial x} + \frac{\partial h v_T}{\partial y} = 0 \ .$$

This latter term arises from the water level elevation set up along the estuary, which can be expanded as

$$\frac{\partial \overline{\zeta_2}}{\partial x} = \frac{1}{g\int_0^D h^2 dy} \qquad \times \Big[2\beta \int_0^D \overline{\zeta_1 u_1} dy - \int_0^D h^2 \big(\overline{u_1 \frac{\partial u_1}{\partial x}} + \overline{v_1 \frac{\partial u_1}{\partial y}} dy\big)\Big].$$

The solutions presented above differ from those in Li & O'Donnell on the order of ϵ on terms 3 and 4 of equations (13) and (15). To continue our study of short, low-inflow estuaries, will use the solution forms as presented in Li & O'Donnell, 2005 to continue this work and to simulate case study conditions.

$$u_T = 2\overline{\frac{\zeta_1 u_1}{h}} + -\frac{h}{\beta}\Big(\overline{u_1\frac{\partial u_1}{\partial x}} + \overline{v_1\frac{\partial u_1}{\partial y}}\Big) + -\frac{gh}{\beta}\frac{\partial\overline{\zeta_2}}{\partial x} \tag{16}$$

with

$$u_{T1} = 2\overline{\frac{\zeta_1 u_1}{h}} \qquad u_{T2} = -\frac{h}{\beta}\Big(\overline{u_1\frac{\partial u_1}{\partial x}} + \overline{v_1\frac{\partial u_1}{\partial y}}\Big),$$

$$u_{T3} = -\frac{gh}{\beta}\frac{\partial\overline{\zeta_2}}{\partial x}.$$

Here, u_{T1} describes Stokes transport, u_{T2} describes advection along the system, and u_{T3} describes the baroclinic pressure gradient, and the resulting return flow.

Thus, the solutions for axial and lateral transport velocities to be used to simulate the case study are:

$$u_T = 2\overline{\frac{\zeta_1 u_1}{h}} + -\frac{h}{\beta}\Big(\overline{u_1\frac{\partial u_1}{\partial x}} + \overline{v_1\frac{\partial u_1}{\partial y}}\Big) + -\frac{gh}{\beta}\frac{\partial\overline{\zeta_2}}{\partial x}$$

$$v_T = 2\overline{\frac{\zeta_1 v_1}{h}} + -\frac{h}{\beta}\Big(\overline{u_1\frac{\partial v_1}{\partial x}} + \overline{v_1\frac{\partial v_1}{\partial y}}\Big) + -\frac{gh}{\beta}\frac{\partial\overline{\zeta_2}}{\partial y}$$

$$h\frac{\partial u_T}{\partial x} + \frac{\partial h v_T}{\partial y} = 0.$$

CHAPTER 4

UNDERSTANDING VOLUME TRANSPORT

From the model developed by Li & O'Donnell 2005, the tidal characteristics of the Jordan River have been investigated to help understand sub-tidal flows and transport. The parameters for the Jordan River used to inform the model are L length, D width, T tidal period, U_0 amplitude of along channel velocity, A_0 amplitude of water level elevation and $h(y)$ bathymetry. We will run the model using the observed parameters from the study site.

4.1 Data Analysis

4.1.1 Bathymetry

The restriction that the model places on the cross-sectional profile is that it is sufficiently smooth (we used a moving average in this analysis) and differentiable. This means that irregularities in the bottom profile such as shoals (shallower areas near the landward boundaries) and channels (deeper portions nearer the center) will not affect the solution form granted that they are differentiable (sufficiently smooth), and thus irregular and highly specified bathymetric profiles can be modeled with these solutions.

We can then use profiles collected from ADCP transect data, which includes a bottom profile with each pass (27 transects). These are smoothed using a moving average across the profile. The left-hand side is the east bank of the estuary, and the right-hand ride is the west bank (the perspective of the profile is looking seawards). In order to capture the furthest cross-sectional extent of the bathymetry, profiles were chosen from the collection at the times of highest tide. A simple smoothing gives us results that can be prescribed for $h(y)$.

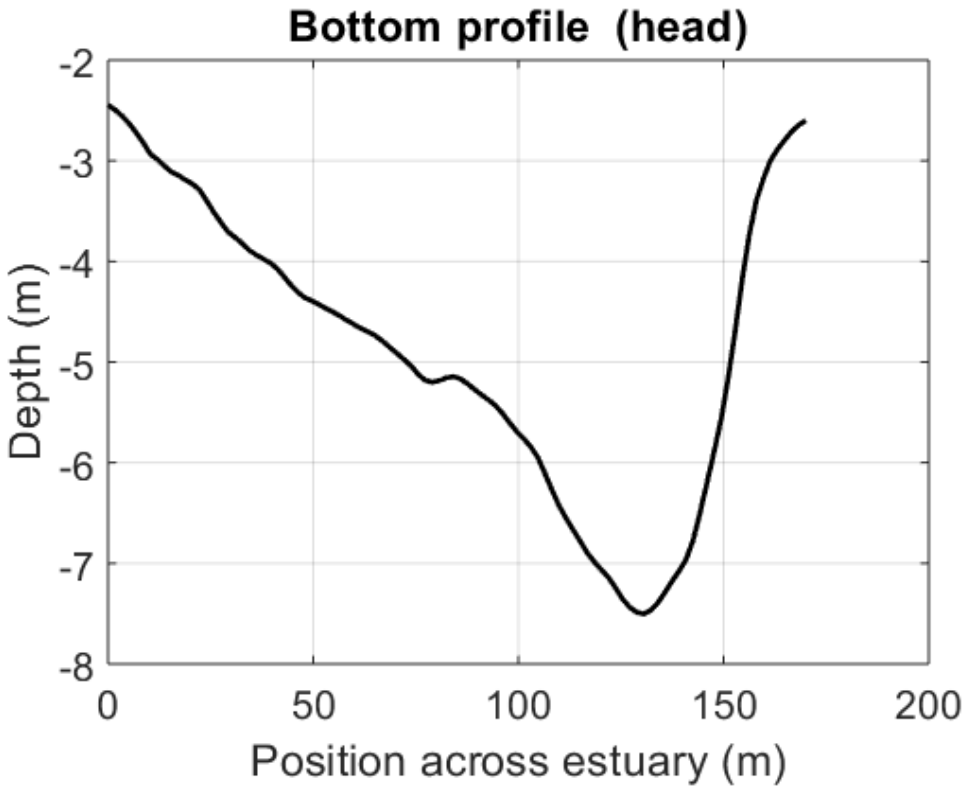

Figure 6: Bottom profile for the transect nearest the head. Perspective is looking seaward, with the left side of the profile being the eastward bank, and the right side being the westward bank of the Jordan River.

4.1.2 Salinity Structure

In making the assumptions necessary to derive system-specific equations for tidally forced velocity, it is necessary to identify the salinity structure of the system for the given freshwater inputs. Salinity contours from the CTD profiles in the middle of each transect are plotted against time (during one tidal cycle) in figure 7. From this, we can see that there is little variation with depth (the highest being only 0.2864 ppt difference throughout the water column). For reference, the tidal variation was 1.1611 ppt (with ocean water typically measuring at 35 ppt). This allows us to classify this system as well-mixed, for the season and conditions under which these data were collected (Valle-Levinson, 2001).

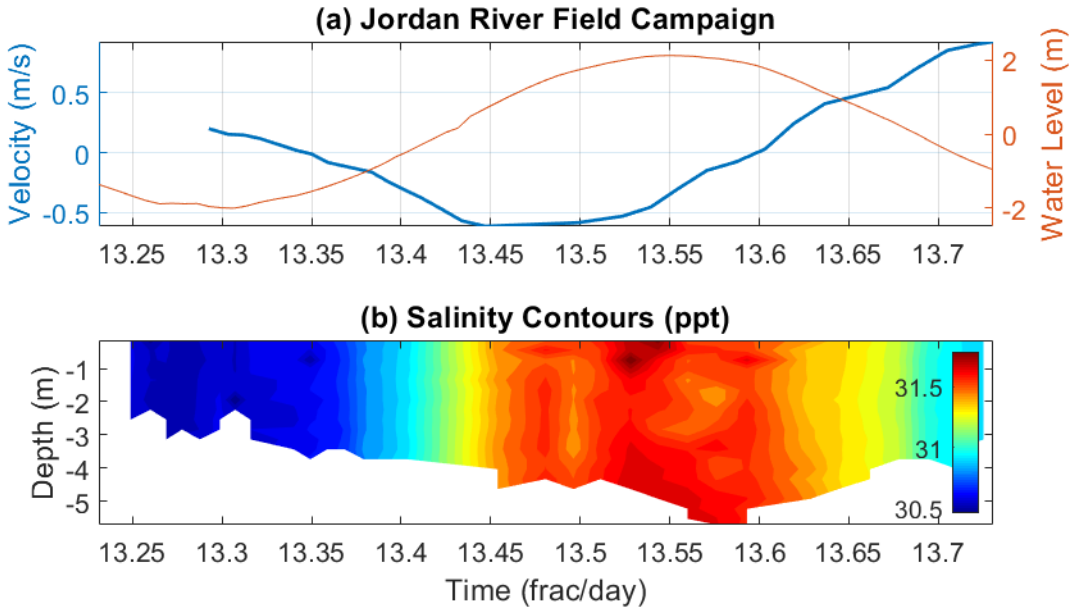

Figure 7: Results of CTD and averaged velocity data analysis. Amplitude of axial velocity (figure a, blue), water level (figure a, orange), and Salinity contours (figure b) shown for one tidal cycle during ADCP sampling. Note that there is little salinity variation with depth.

4.1.3 Water Level

In order to quantify the amplitude of water level elevation, the amplitude of the tidally forced water level was isolated from the least squares fit of the pressure sensor data, giving us the following results from each station. We will use the representative mean of M2 harmonic amplitudes to assign the for tidal water level amplitude $A_0 = 1.528$ meters as seen in figure 8.

η	M2	M4	M6	ζ'
Mouth	1.526	0.0237	0.0015	-0.0147
Mid	1.528	0.0269	0.0092	-0.0149
Head	1.530	0.0293	0.0077	-0.0149

Figure 8: Results of least squares fit of water level data at 3 pressure sensor stations (mouth, middle, and head). The M2, M4, and M6 columns denote the amplitude of each respective tidal constituent at each location in meters, and ζ' denotes the estimated residual water level elevation at each location in meters.

4.1.4 Velocity

In order to quantify the amplitude of axial velocity for a semi-diurnal tidal cycle, a least squares fit was performed on the velocity profile data. Because continuous samples were collected for a period of just under a full tidal cycle for Frenchman Bay (12.42 hours), a theoretical wave can be fit to the data. This is then used to isolate the influence of each tidal harmonic.

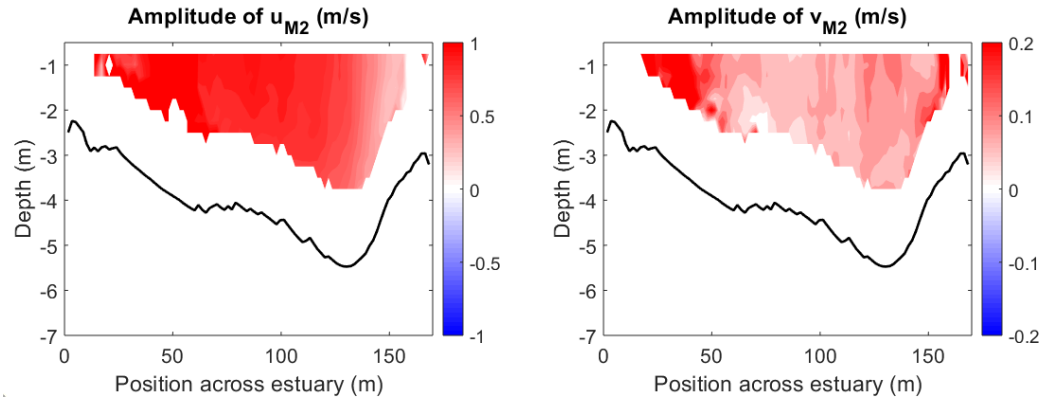

Figure 9: Results of the least squares fit isolating the amplitude of the tidally forced axial velocities (U_{M2}) and amplitude of lateral velocities (V_{M2}).

This fit considered M_2, M_4 and M_6 constituents, with periods of 12.42, 6.21, and 4.14 hours respectively. From this we can isolate U_0 and the residual velocities measured (those not accounted for by the three harmonics).

The amplitude of tidally driven axial flow (U) and lateral flow (V) are the respective amplitudes of the M_2 harmonic. This gives us an across channel and depth mean of the values as $U = 0.8201^{m}/_{s}$ and $V = 0.1456^{m}/_{s}$, rotated to the primary axis. The variations with depth and position across channel can be seen in figure 9. Generally, the highest axial velocities are seen over the deepest part of the channel, and the lowest over the shoals.

U	V	L	D	ζ_0	T
0.8201 $^m/_s$	0.1456 $^m/_s$	4880 m	170 m	1.528 m	12.42 hours

Figure 10: Parameters and model inputs specific to study site calculated from *in situ* data. All values are constant to be used in previously derived solution form.

4.2 Subtidal Flows and Transport

The following are results from the depth averaged model presented above based on Li & O'Donnell 2005, with appropriate parameters for the Jordan River (see figure 10). The model was run for the values observed at transect 1, nearer the head (see figure 1). This was because transect 1 better represented the morphology of the system throughout. Transect 2 traversed a tidal flat on the western edge of the channel, potentially affecting the flow. Using the bathymetry and tidally driven amplitude parameter (U_0), the model presents an idealized distribution (along and across the system) of U (the amplitude of along channel velocity as it varies throughout the system). Axial velocity is dampening along the channel, as expected. This is because frictional effects cause the tidal wave to slow as it travels up estuary.

Additionally, modeled second order equations for axial velocity (13), or transport velocity, with each constituent ($u_{T1},\ u_{T2}$, and u_{T3}) are shown in Figure 11. From this, the first plots represent the contributions of $u_{T1} = 2\dfrac{\overline{\zeta_1 u_1}}{h}$. This term describes Stokes drift, or the movement of particles due to the interaction between the tidal wave and bottom friction or the net movement resulting from the variation in speed of propagation of the tidal wave from crest to trough. We can see that this mechanism is causing net inflow over the channel and net outflow over the shoals (see figure 11). This is due to our zero-flux boundary condition at the head.

Momentum advection is described by $u_{T2} = -\dfrac{h}{\beta}\Big(\overline{u_1\dfrac{\partial u_1}{\partial x}} + \overline{v_1\dfrac{\partial u_1}{\partial y}}\Big)$. There is net inflow across the channel, though the magnitude sharply increases over the deepest portions of the channel, and nearer to the mouth. This pattern aligns with our

definition of advection as a result of axial flow, and not a driver of flows intrinsically. Where there is faster flow (over the channel) there will be more powerful advection. Because of the narrow nature of the channel, we suspect that this term is dominated by along channel gradients in tidally driven velocities, as opposed to cross channel gradients.

Finally, $u_{T3} = -\frac{gh}{\beta}\frac{\partial \overline{\zeta_2}}{\partial x}$ describes subtidal flows induced by an along channel baroclinic pressure gradient set up. This is consistently negative (denoting outflow) across the channel, which ties in well to our understanding of the system, as baroclinic gradients will always produce an outflow. An along channel pressure gradient is set up when fluid piles up at the head increasing pressure in that region. The fluid tends to travel towards areas of low pressure, thus creating a return flow seaward. The along channel gradient should be positive, thus subtracting this term gives us a consistently negative value throughout.

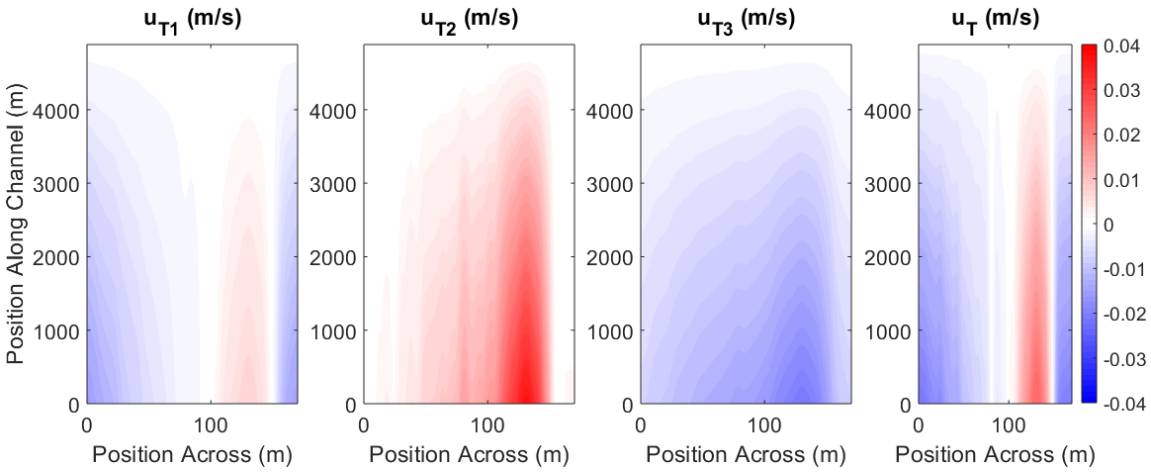

Figure 11: Modeled second order (subtidal) axial velocity in the Jordan River, isolated into three components. Red denotes inflow and blue denotes outflow, while $y = 0$ represents the mouth of the estuary as these plots show an idealized rectangular depth averaged system (as if looking from above).

4.3 Discussion

Though the total value of transport velocity (u_T) appears similar in distribution to Stokes drift (u_{T1}), the value of this first constituent term over the channel is an order of magnitude smaller than that of the final transport. Because the total transport is simply the sum of these parts, we can deduce that Stokes drift is not the main driver of the patterns we are seeing. Instead, the combination between advection (u_{T2}) and pressure gradient (u_{T3}) are a more likely explanation. Advection is the most powerful driver and causes net inflow over the channel to overtake the effects of the pressure gradient. However, advection is a result of first order flux, and highly dependent on depth, thus less influential over the shallower shoals.

It is in this area that the along channel water level elevation set up can take hold. The mass piled at the head of the system must go somewhere. Thus, it is likely that it hits the no flux boundary at the head and is transported seawards. This could be because of the pressure gradient but also the tidal wave characteristics rebounding off the head to produce seaward drift along the sides.

In order to confirm these results with data, our analysis can be compared with the small set of least squares fit values directly above the deepest portion of the channel. The magnitude of the modeled total transport velocity over the channel is about 0.02 $^{m}/_{s}$ at the location of the transect (1156 meters along the channel).

We can see that the mean value of residual velocity at this station are approximately 0.023 $^{m}/_{s}$ over the deepest part of the channel. Similarly, for the model run with parameters from the head, at the theoretical location of the head, we have 0.019 $^{m}/_{s}$ (see Figure 12). The order of magnitude for these transport velocities is the same in both the model and the data. However, both amplitude of axial velocity and transport velocity are lower than expected for the results modeled using parameters from the head.

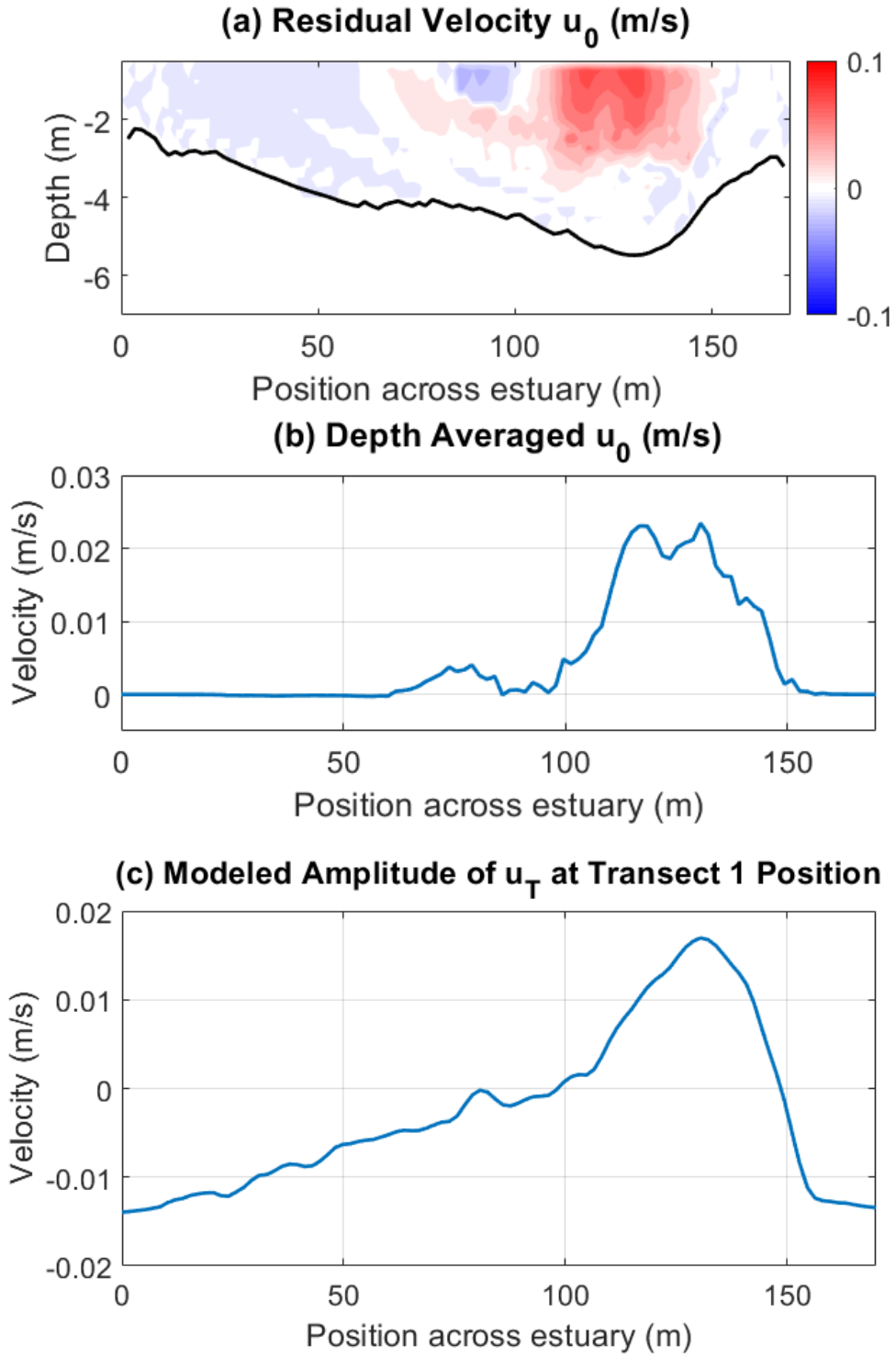

Figure 12: Residual flow in the Jordan River isolated from velocity data collected *in situ* (a). Depth averaged residual velocity at ADCP location (b), and modeled transport velocity at transect location (c).

This model also does not take into consideration the funnel shaped characteristics of the portion of the system directly adjacent to the mouth that could cause a small amplification of the tidal wave, but instead assumes that the cross-channel profile is constant along the channel. The data also shows a lower order of magnitude for the outflow seen of the shallower portions of the estuary. This could be because there were boulders and other irregularities that could affect these velocities. We have assumed a constant bottom drag coefficient (C_D), however conditions in the field are not as idealized as the model must assume.

Additionally, this model assumes that the tidal wave is both progressive in nature and that it undergoes significant dampening as it travels up-estuary. This could also lead to smaller than expected modeled values for the theoretical location of the head transect. Another limitation is the size of the system. It is so small that not only is navigation from bank to bank difficult during low tide, but also that the width of the system changes so drastically throughout a tidal cycle that we cannot calculate least squares fit values anywhere other than directly over the channel. Despite this, we have been able to confirm, to an order of magnitude, that the inflow over the deepest part of the channel is accurate. In this case, there can not only be inflow, but mass must also move out of the system as well.

These results are significant to our study of short, low inflow estuaries as it mirrors the patterns of residual flows modeled in Li & O'Donnell, 2005 in a significantly larger estuary with higher rates of inflow. Despite the differences in system classification, the solution forms retain their overall result pattern. This implies that this solution can be used to model tidal and subtidal flows in systems of varying length, with relatively uniform width and depth along-estuary.

4.4 Gradients

The following modelled solutions and subsequent analysis of flow in the case study area are contingent on the presence of certain physical conditions in the system. These allow for assumptions to be made about the nature of sub-tidal flows in this case. Should a system similar in many ways (non-convergent, shallow, short, and rectangular) exhibit changes in these conditions, we may not see the same patterns of transport.

Quantifying water surface gradients in this system was made difficult due to limitations of measurement equipment. During deployment of the three pressure sensors (see Figure 4), there was an attempt to conduct an elevation survey of their positions. From the measurements, we see that the change along the estuary is not in one direction, indicating an issue with measurements (see Figure 13). We will continue while neglecting the middle reading. A Sokkia CX105 total station was used to sight the positions of the sensors from a fixed point near the location of transect 1. This unit can resolve angles to 5 arc-seconds. If we consider the maximum slope, we can see that this will induce a stronger compensatory flow landwards (with $x = 0$ representing the mouth of the estuary). As we can see from comparing residual flows from the data to model outputs, outflow is weaker along the shoals than predicted (see Figure 12). This suggests that there is a hindrance to the outflow across the system and may dampen the effects that are induced by u_{T1} and u_{T3}. Because the distance to the sensors was at times quite significant (approximately 1 km for the location near the head, and 0.5 km for the location near the mouth), this lead to an error in the elevation that was quite large compared to the expected change in water level (2.5 cm at the longest sight), because the system is so small as to not exhibit a significant slope.

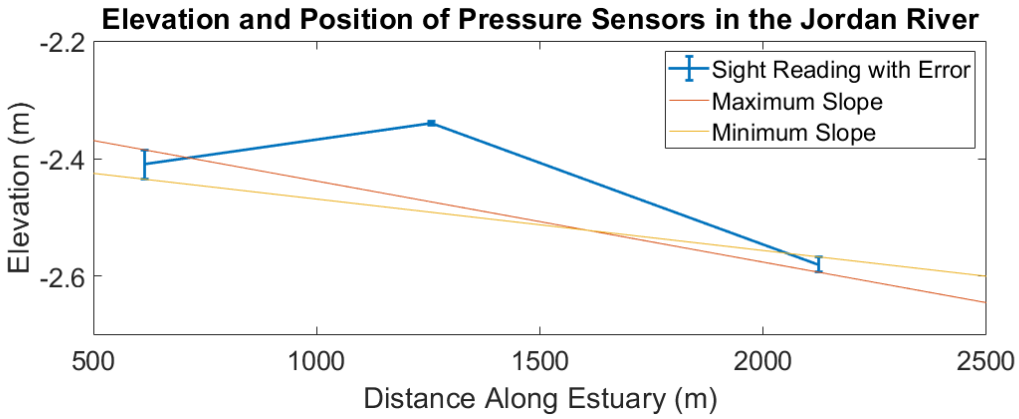

Figure 13: Measured position and instrument error of pressure sensors deployed in the Jordan River. Neglecting the middle reading, the red line represents the maximum slope allowable considering error, and the yellow represents the minimum.

The data collection period in the Jordan River was during the dry season, where river discharge was extremely low, so much so that we were able to dismiss its contribution to flow. The system was classified as well-mixed, and thus density gradients were not considered. If this study is repeated in another system, or during the wet season in the Jordan, this may change. If river discharge is high enough, we could see patterns of vertical circulation appear. We were able to show that the vertical gradient of salinity was negligible in this system (or that salinity does not change significantly with depth). If sufficient discharge of lighter, less saline water enters at the head, this could cause increased vertical stratification, and form an area of outflow on the surface, with compensatory inflow at depth (Pritchard, 1952). This changes the pattern of sub-tidal velocity, and also prohibits the use of the model and solutions obtained in chapter 3. Additionally, this pattern has a vertical component to the circulation, which could not be captured by this model because the solutions are depth averaged.

Temperature differences, and the further changes in density that this can cause were also not considered in this study. However, there is potential for this to become increasingly relevant given the advance of climate change. The Gulf of

Maine is warming more rapidly than 99.9% of the rest of the ocean (Pershing et al, 2015). In the future, temperature gradients may arise should warmer, lighter ocean waters meet cold, dense snow melt in estuarine systems. This could introduce patterns of vertical circulation, with these density differences counteracting the effects of salinity in terms of typical estuarine circulation. Also, the field campaign was conducted at a midpoint between spring and neap tide. Spring tide, with a larger tidal range, produces more intense tidal velocities. These then increase sub-tidal velocities in similar tidally dominated systems, and thus pollutant matter could spend less time suspended in the system during this period of the tide (the opposite occurring during full neap tide). Keeping these differences in mind, we can postulate the changes to the patterns that we see here should the model be applied to similar systems in future case studies.

CHAPTER 5

CONCLUSIONS

The purpose of this study was to be able to characterize the residual circulation patterns in an idealized domain of a dynamically small system. Our model indicates residual inflow over the channels and residual outflow over the shoals. This can be explained by a combination of axial advection and pressure gradient force. Advection acts primarily landwards, however, because our model approximates the morphology of the system using a semi-enclosed basin, the tidal wave may be reflected off of the closed end and continue to propagate seawards over the shoals (away from the competing inward advective influence). Because of our boundary conditions, the model does not account for this. Once reflected, baroclinic pressure gradients amplify this seaward movement, creating net transport outwards over the shoals.

From the least squares fit applied to the velocity data collected at the Jordan River, we can see that the maximum value of axial residual flows is 0.0791 $^{m}/_{s}$. From the model output, the maximum value for total transport (u_T) is 0.0248 $^{m}/_{s}$. These values are of the same order of magnitude, indicating recreation of general trends within the system, subject to further validation.

In terms of aquaculture management, the pattern of residual velocity that we see in this model indicates shorter pollutant exposure periods. Should pollutants (either derived from runoff of a point source) enter the system through the small river at the head or through outlets along the shore, the results of the model run show that the material will be transported out of the system through the shoals, as opposed to traveling landwards through the shoals, to then later leave through the channel. Further study is needed on the path of ocean-derived pollutants residence within

estuarine systems should the future hold promises of offshore drilling off the eastern coast of the United States. We can see from this model that pollutants entering this system from the seaward boundary have a longer path within the system due to the pattern of residual flows. In this case, both seabed and wild shoal mussels, as well as fauna within the water column and throughout the seabed are at an increased risk due to the higher axial velocities generally seen over deeper portions of a system.

References

Andersen O.B. (2003) The M4 Shallow Water Tidal Constituent from Altimetry and Tide Gauges. In: Hwang C., et al (eds) *Satellite Altimetry for Geodesy, Geophysics and Oceanography. International Association of Geodesy Symposia*, vol 126. Springer, Berlin, Heidelberg

"Bar Harbor, ME - Station ID: 8413320. Tides & Currents", *The National Oceanic and Atmospheric Administration (NOAA)*, 2018, tidesandcurrents.noaa .gov/stationhome.html?id=8413320.

Burchard, Hans, et al. Drivers of Residual Estuarine Circulation in Tidally Energetic Estuaries. *Journal of Physical Oceanography*, vol. 41, no. 3, 2011, pp. 548-570., doi:10.1175/2010jpo4453.1.

Cameron, W. M. and D. W. Pritchard (1963) *Estuaries*. In M. N. Hill (ed.), The Sea , Vol. 2. John Wiley Sons, New York, pp. 306-324.

Chen, Shih-Nan, et al. Estuarine Exchange Flow Quantified with Isohaline Coordinates. *Journal of Physical Oceanography*, 6 Nov. 2011.

Dronkers J. (1986) Tidal Asymmetry and Estuarine Morphology. *Netherlands Journal of Sea Research* 20, 117-131.

Friedrichs, Carl T. Barotropic Tides in Channelized Estuaries. *Contemporary Issues in Estuarine Physics*, edited by Arnoldo Valle-Levinson, Cambridge University Press, 2010, pp. 27-61.

W. Geyer & P. MacCready. (2014). The Estuarine Circulation. *Annual Review of Fluid Mechanics* 46, 175-197.

Huijts K. et al (2011) Transverse structure of tidal and residual flow and sediment concentration in estuaries. *Journal of Ocean Dynamics* 61, 1067-1091.

Huijts et al. (2009) Analytical study of the transverse distribution of along-channel and transverse residual flows in tidal estuaries. *Continental Shelf Research* 89-100.

Joyce, T. M.(1989). *In situ* calibration of ship-board ADCPs. *Journal of Atmospheric and Oceanic Technology*, 99, 20445-20461.

Li & O'Donnell. (2005) The Effect of Channel Length on the Residual Circulation in Tidally Dominated Channels. *Journal of Physical Oceanography* 35, 1826-1840.

Li & Valle-Levinson. (1999) A two-dimensional analytic tidal model for a narrow estuary of arbitrary lateral depth variation: The intratidal motion. *Journal of Geophysical Research* 104, 23525-23543.

Parker, B.B. (1984) Frictional effects on the tidal dynamics of a shallow estuary (Doctoral Dissertation, Johns Hopkins University). 292 pp.

Pershing, A. et al (2015) Slow adaptation in the face of rapid warming leads to collapse of the Gulf of Maine cod fishery. *Science* 350, 809-812.

Pritchard, D. W. (1952) Estuarine hydrography. *Adv. Geophys.* 1 , 243- 280.

Pritchard, D. W. (1956) The dynamic structure of a coastal plain estuary. *Journal of Marine Research* 15(1), 33-42.

Thomson, R. E., & Emery, W. J. (2014). Data analysis methods in physical oceanography (3rd ed.). Waltham, MA: Elsevier.

Valle-Levinson, Arnoldo. Definition and classification of estuaries. *Contemporary Issues in Estuarine Physics*, edited by Arnoldo Valle-Levinson, Cambridge University Press, 2010, pp. 27-61.

Viarengo & Canesi. (1991) Mussels as biological indicators of pollution. *Aquaculture* 94 225-243

Warner J. et al (2005) Numerical modeling of an estuary: A comprehensive skill assessment. *Journal of Geophysical Research:* Oceans 110, https://doi.org/10.1029/2004JC002691

Author's Biography

Gwyneth E. Roberts was born in Portland, Maine on May 18, 1996. She was raised in Cape Elizabeth, Maine. Gwyneth has earned dual degrees, a B.A. in Mathematics and a B.S. in Environmental Sciences. She is a member of Phi Kappa Phi, Pi Mu Epsilon, and SPIRE: The Maine Journal of Conservation and Sustainability. She has received a George J. Mitchell Center for Sustainability Solutions award for Outstanding Contribution to Sustainability Research for this project. Upon graduation, Gwyneth plans on starting a career in renewable energy.